MEASUREMENT OF POWER SYSTEM SUBSYNCHRONOUS IMPEDANCES AND COMPARISON WITH COMPUTER SIMULATIONS

By

MICHAEL BRENT HUGHES

B.A.Sc., The University of British Columbia, 1975

A THESIS SUBMITTED IN PARTIAL FULFILLMENT OF

THE REQUIREMENTS FOR THE DEGREE OF

MASTER OF APPLIED SCIENCE

in

THE FACULTY OF GRADUATE STUDIES

Department of Electrical Engineering

We accept this thesis as conforming

to the required standard

THE UNIVERSITY OF BRITISH COLUMBIA

November 1984

In presenting this thesis in partial fulfilment of the requirements for an advanced degree at the University of British Columbia, I agree that the Library shall make it freely available for reference and study. I further agree that permission for extensive copying of this thesis for scholarly purposes may be granted by the head of my department or by his or her representatives. It is understood that copying or publication of this thesis for financial gain shall not be allowed without my written permission.

Department of ELECTRICAL ENGINEERING

The University of British Columbia
1956 Main Mall
Vancouver, Canada
V6T 1Y3

Date 18 DEC 1984

ABSTRACT

A test method is developed to measure the equivalent (driving point) positive sequence impedance, as a function of frequency, of an operating power system. The technique used is to apply a phase-to-phase fault at the system node of interest and record the transient voltage across and current in the fault. These quantities are then transformed into the frequency domain. The system driving point impedance is then taken as the ratio of the fault voltage to the current at each point in the frequency domain. Field results from a phase-to-phase fault at a central location on the B.C. Hydro 500 kV network are presented and analysed to determine the system driving point impedance. The measured impedance versus frequency characteristic is compared with a predicted impedance characteristic based on an Electro-Magnetic Transient program study of a detailed model of the major B.C. Hydro transmission and generation. Correlation between the measured and calculated impedance is good, with explanations offered for any localized significant disagreement. The explanations offered are subsequently verified by Ontario Hydro's improvements to the analysis of the test data and additions to the computer model data.

Table of Contents

List of Figures

ACKNOWLEDGEMENTS

The author would like to acknowledge his colleages Messrs. T.G. Martinich and R.W. Leonard as equal partners in the work presented herein and express his gratitude for their generous consent to its use in this thesis.

The author is very grateful to the System Planning Department of British Columbia Hydro for its encouragement, cooperation and support for this project in particular and for the Masters Degree program in general. The flexibility shown was instrumental in allowing the author's studies to proceed while remaining employed, full-time, with B.C. Hydro.

Special thanks are due to Messrs. Y. Mansour, M. Scott, J.H. Sawada, and M.G. Bradwell (retired), of B.C. Hydro for their valuable discussion and advice during the preparation of this thesis, and to Mr. Sawada and Dr. A. Morched of Ontario Hydro for permission to include their significant improvements to the initial work.

The author would like to thank Dr. L.M. Wedepohl as co-reader of this thesis. And finally, the author would like to express his sincere appreciation to Dr. H.W. Dommel for his most valued guidance and support as instructor, and M.A.Sc. program and thesis supervisor.

1 INTRODUCTION

The present B.C. Hydro power system is based almost entirely on hydroelectric generation on the Peace River and Columbia River systems. This generation is connected by a network of 500 kV transmission lines to the lower mainland and Vancouver Island, the main load centers of the province (Figure 1). In the case of the Peace River generation, series capacitors are used to increase the power transfer capabilities of the 500 kV transmission lines.

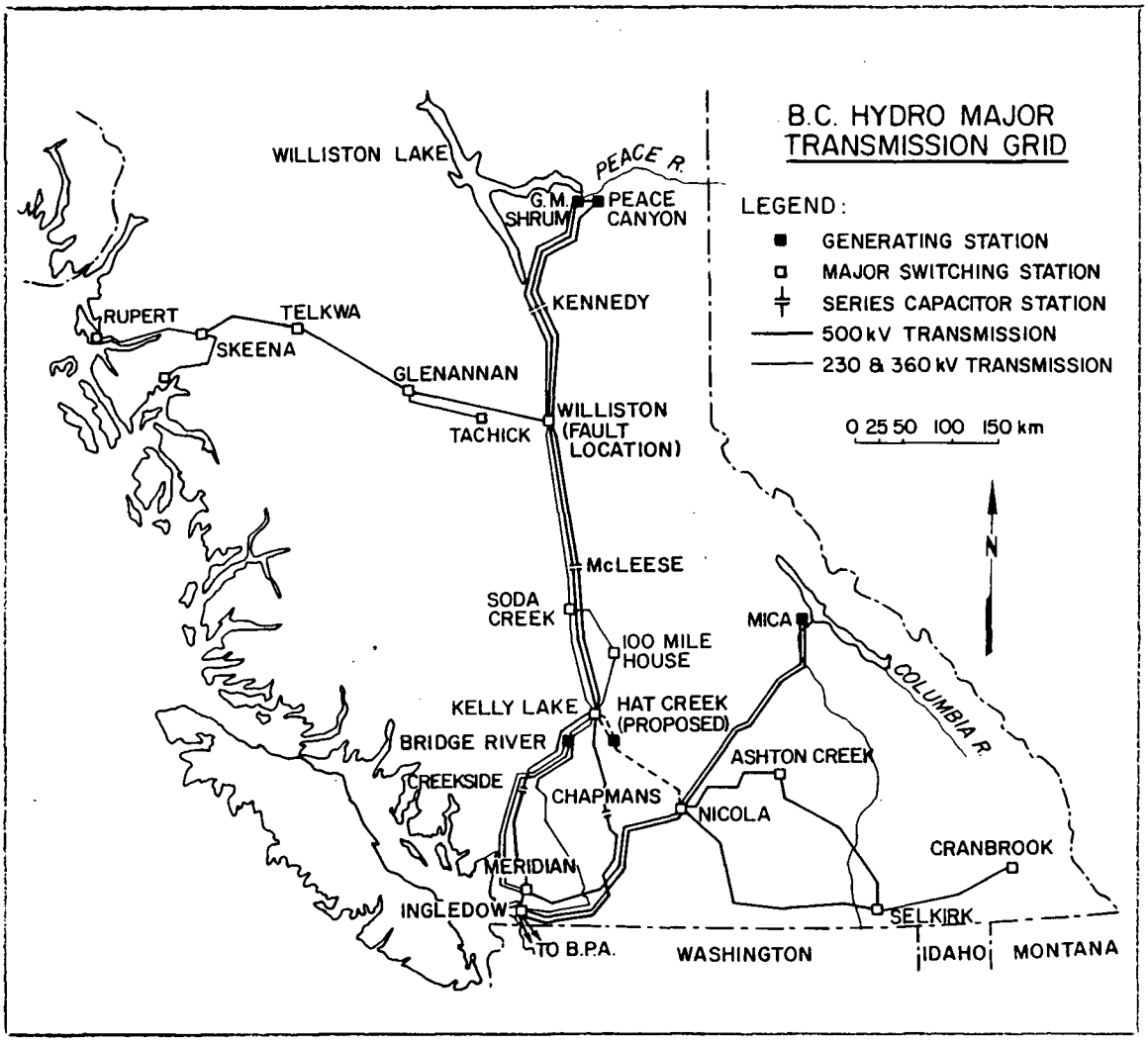

FIGURE 1 - B.C. HYDRO MAJOR TRANSMISSION SYSTEM

Until recently, long range plans included the addition of a large

coal-fired thermal generating station at Hat Creek that was to be incorporated into the existing 500 kV transmission system. Operating experience in the southwestern United States [1] has shown that, under certain circumstances, there can be unstable electrical oscillations in the generation and transmission system that can induce destructive mechanical oscillations on the shafts of steam powered turbine generators. These oscillations can occur if there is a correspondence between an electrical transmission system resonant frequency, due to the series capacitors in series with the transmission line reactance, and a mechanical torsional resonant frequency of the various turbine and generator components on a common shaft. This phenomenon is now referred to as sub-synchronous resonance (SSR) and was responsible for two destructive events at the Mohave Generating Station in the U.S.A. in 1970 and 1971. It was therefore very important to assess the possibility of SSR occuring with the proposed Hat Creek generator connected to the center of a series compensated 500 kV transmission system.

Various methods of analyzing and predicting the occurence of SSR had been developed and are reported in the literature. The method adopted by B.C. Hydro is explained in reference [2]. One of the key pieces of data required for this analysis was knowledge of the positive sequence equivalent impedance of the electrical system as a function of frequency, $Z_{pos}(jw)$, at the point of connection of the generating station. In particular, the system subsynchronous resonant frequencies (those below the 60 Hz system frequency) and the resistance offered at those frequencies, must be known. This data is not generally available within power utilities. A detailed Electromagnetic Transients Program (EMTP) [3] model of the 500 kV transmission system was therefore constructed to derive this information.

The system impedance frequency spectrum was derived for the EMTP model

developed however there was no measured data with which to validate it. There were no industry standard tests that would measure $Z_{pos}(jw)$ and a literature search done in early 1981 indicated that this had not previously been done. Given that subsynchronous resonance countermeasures would or would not be installed based on the results of these SSR studies, it was essential that the impedance data used was accurate. If erroneous impedance data led to a decision not to install countermeasures and they were in fact required, the consequences could be broken turbine generator shafts and a lengthy generating plant outage followed by output curtailments while countermeasures were being retrofitted. If erroneous impedance data led to generator design changes and installation of countermeasures that were in fact not required, millions of dollars would have been wasted. It was therefore decided to develop some means of measuring the system impedance as a function of frequency.

2 MEASUREMENT TECHNIQUE

2.1 Theory

Two general methods of measuring the system impedance were considered. These methods were essentially variations of methods which have been used successfully for measuring transfer functions of control systems such as in exciters and power system stabilizers. The first was a discrete sinusoid or steady state technique [4]. In theory, the impedance is obtained by sequentially applying positive sequence currents at discrete frequencies into the system and recording the steady state voltages produced as a response to the input. The ratio of the magnitudes of voltage to current and the phase angle difference between the two at each frequency determines the driving point impedance (Figure 2). The

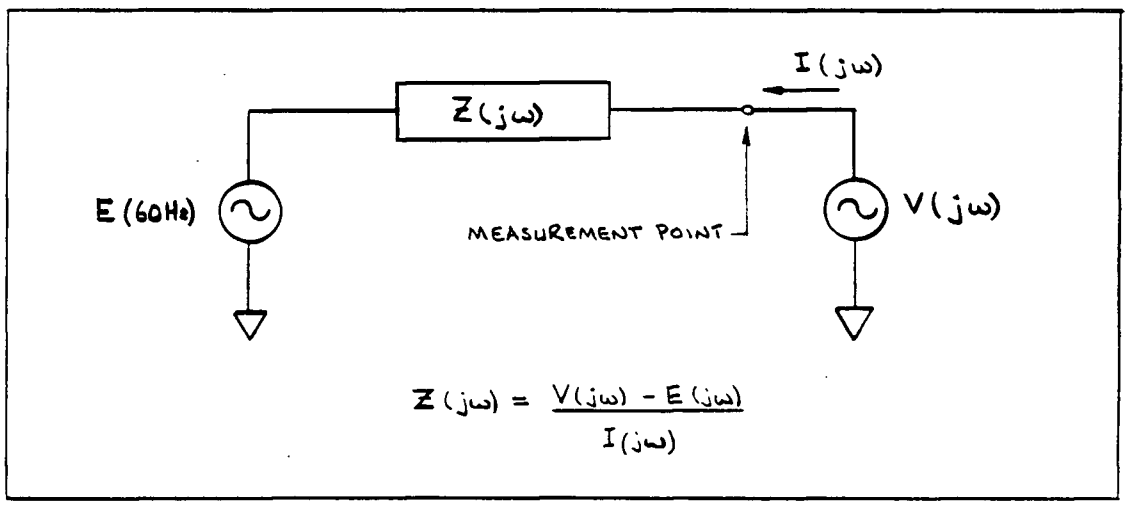

FIGURE 2 - IMPEDANCE MEASUREMENT BY DISCRETE FREQUENCY CURRENT INJECTION

injection could be done at the tertiary windings of a 500/230 kV auto-transformer. For an adequate frequency coverage, a large number of separate measurements would be necessary, thus making the technique time consuming. The idea was rejected because:

(1) it would be difficult to couple a variable-frequency source into an energized high voltage transmission system,

(2) power frequency voltages and currents would be so much greater than the injected signals that severe filtering and dynamic range requirements would be imposed on the test instrumentation, and,

(3) the system configuration would have to remain constant during the course of the measurements.

The second general method considered was the injection of noise current signals [5,6,7,8], with wide spectral content, into the system and the continuous recording of the voltage response along with the current input (Figure 3). By digitizing the recorded waveforms and calculating

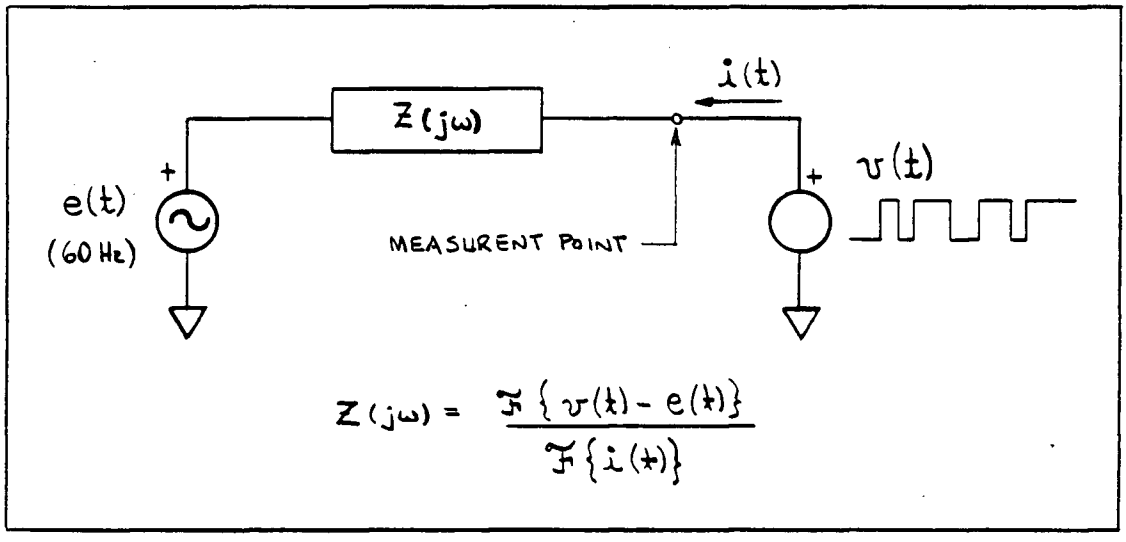

FIGURE 3 - IMPEDANCE MEASUREMENT BY NOISE INJECTION

their Fourier transforms, the system impedance, Z(jw), could then be found as before. The injection point would again be at a transformer tertiary. In practice, however, the idea suffers from problems (1) and (2) mentioned above. There were no naturally occuring disturbances that could be used as the current input [5,7,8,9] and it was estimated that for a 1 kW signal input (the maximum attainable with the test equipement on hand) the

voltage to be measured would be about 115 db down from the 60 Hz component and therefore extremely difficult to detect.

Although the noise signal technique was rejected, a variation of the idea seemed more promising and was studied. Abrupt system changes, such as applying and clearing system faults, generate transient voltages and currents having components over a wide range of frequencies including the subsynchronous region. The theory of compensation states that the application of a fault could be represented as a change in the system impedance or as an injection of the fault current into the unfaulted network (Figure 4). If the later view is adopted then the system

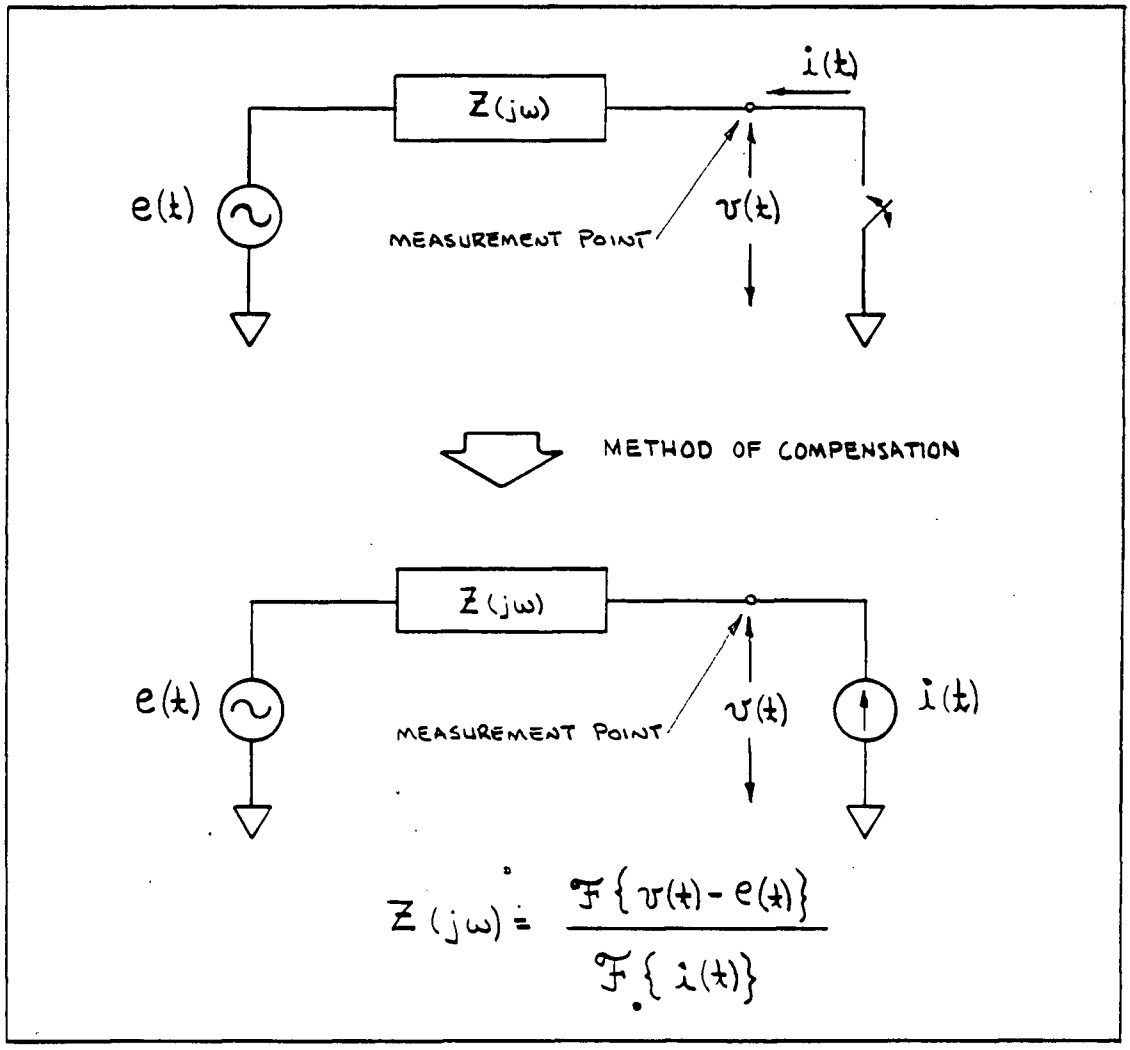

FIGURE 4 - IMPEDANCE MEASUREMENT BY SYSTEM DISTURBANCE

impedance can again be derived as the ratio of the Fourier Transforms of the voltage and current transient waveforms.

2.2 Application to Three Phase Network and Zpos

In extending this concept to a three phase network and the positive sequence impedance, there are various types of fault to be considered. Some generate positive sequence components; some generate positive and negative sequence; and others generate positive, negative and zero sequence [10]. A single phase-to-ground fault was ruled out because it produces equal amounts of positive, negative, and zero sequence currents. These currents essentially flow in the series connection of the positive, negative and zero sequence equivalent networks. It would not be possible to deduce directly the positive sequence network from this type of fault. A simultaneous three-phase fault, in theory, is ideal in that only the positive sequence network and positive sequence current is involved - no negative or zero sequence is present. However, in practice the three poles of the circuit breaker applying and clearing such a fault will not do so simultaneously. This is due to mechanical constraints producing pole scatter and the fact that each pole will interrupt at a current zero. Zero sequence currents would therefore be produced, making this type of fault also unacceptable.

The possibility of using a phase-to-phase fault to stimulate subsynchronous currents was examined. Phase-to-phase fault current consists of practically equal amounts of positive and negative sequence currents. Appendix I shows that if a balanced system is assumed, the steady-state phasor relationship between the voltage across and the current in a phase A to B fault, at system frequency, is:

$$V_{ab} - E_{ab} = (Z_{pos} + Z_{neg})\, I_f \qquad (1)$$

If it is further assumed that the positive and negative sequence impedances are equal, which is true for all passive network components (lines, reactors, capacitors, transformers), then the above steady-state equation becomes:

$$Z_{pos} = \frac{1}{2} \frac{V_{ab} - E_{ab}}{I_f} \qquad (2)$$

A phase-to-phase fault is therefore suitable as a positive sequence excitation source and $Z_{pos}(jw)$ can be calculated as:

$$Z_{pos}(jw) = \frac{1}{2} \frac{\mathcal{F}\{v_{ab}(t) - e_{ab}(t)\}}{\mathcal{F}\{i_f(t)\}} \qquad (3)$$

2.3 Limitations and Practical Considerations

Application of a bolted phase-to-phase fault is a severe system disturbance. The feasibility of using a limited fault to reduce the fault severity was investigated. The only equipment available to limit the fault current was a wye-connected, grounded neutral, three phase line reactor. A limited phase-to-phase fault could be created by applying only two phases of the reactor with the neutral point ungrounded. Unfortunately, this reactor arrangement would overstress the reactor neutral insulation. A bolted phase-to-phase fault was the only practical disturbance left available for this test.

One limitation that is apparent from equation (3) is that if the fault current $I_f(jw)$ is zero at any frequency, then nothing can be said about $Z_{pos}(jw)$ at that frequency. To try and derive $Z_{pos}(jw)$ would be to divide by zero.

Another limitation is that open circuit voltage $e_{ab}(t)$ is not measurable once the fault has been applied. $e_{ab}(t)$ is equal to $v_{ab}(t)$ before the fault is applied. Based on the assumption that the fault will not be severe enough to cause $e_{ab}(t)$ to change, the pre-fault $e_{ab}(t)$ is continued (with the same frequency and magnitude) into the fault and post-fault time periods.

A further point to note about equation (3) is the way the numerator, defined here as the fault voltage $V_f(jw)$, is calculated. The open circuit voltage can be subtracted from the phase-to-phase voltage in the time domain

$$V_f(jw) = \mathcal{F}\{v_{ab}(t) - e_{ab}(t)\} \tag{4}$$

or in the frequency domain

$$V_f(jw) = \mathcal{F}\{v_{ab}(t)\} - F\{e_{ab}(t)\} \tag{5}$$

Both are correct, however, the time-domain formulation will yield a better representation for $V_f(jw)$ for the following reasons. First, only the transient component of the fault voltage contains information about $V_f(jw)$. By doing the subtraction in the time-domain it should be readily apparent what portion of the recorded data should be transformed to the frequency domain. The minimum time will be just before the fault is applied, which corresponds to steady-state conditions and $v_f(t)$ is zero. The maximum time will be when the transient has decayed to zero and steady-state conditions have returned - i.e. $v_f(t)$ is zero again. This leads to the second advantage. Since $v_f(t)$ is zero at the beginning and end of the time interval being transformed to the frequency domain, there is no truncation of the time signal which could cause spurious ripples in $V_f(jw)$ known as Gibbs oscillations [11].

As a check on the impedance measurement technique, the equivalent impedance of an EMTP model of the B.C. Hydro 500 kV system was derived in two different ways and compared.

(1) A phase-to-phase fault in an EMTP power system model was simulated and $Z_{pos}(jw)$ "measured" according to the impedance measurement technique.

(2) All voltage sources (generators) in the model were set to zero magnitude and one Amp of positive sequence current was injected into the system where the fault had previously been. The resulting steady-state, positive sequence voltage at the point of current injection is a direct measure of the system impedance at the current source frequency. Using the frequency scan feature of the EMTP the frequency of the current source was sequentially incremented and the steady-state solution recalculated to form the calculated system impedance. This process is referred to hereafter as the system impedance frequency scan.

Figure 5 compares the two system impedances derived as described above. The extremely close agreement confirms the validity of the impedance measurement technique.

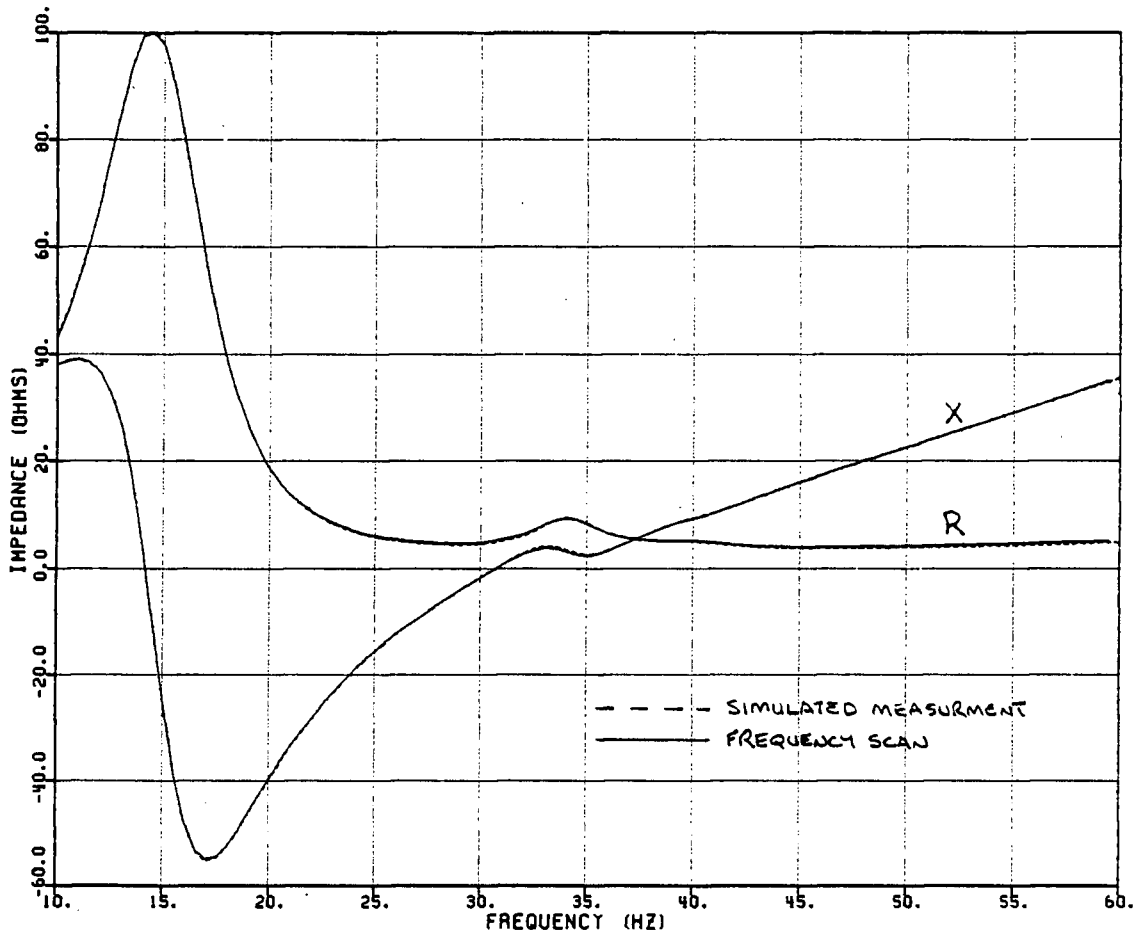

FIGURE 5 - SIMULATED IMPEDANCE MEASUREMENT TEST RESULTS COMPARED WITH IMPEDANCE FREQUENCY SCAN OF THE SAME SYSTEM MODEL

2.4 Validity of Assumptions

The assumption that the positive sequence and the negative sequence network driving point impedances being equal is reasonable. The negative sequence impedance is identical to the positive sequence for all non-rotating power system components. Even for synchronous machines, this is a good approximation over the frequency range of interest. For synchronous machines, considering the 10 to 50 Hz frequency region, the positive sequence operational inductance approximately corresponds to L''_d, as shown by actual test measurements [12,13]. This is particularly true

for salient-pole machines having pole face damper windings, such as for G.M. Shrum and Peace Canyon, where L''_d is fairly constant over these frequencies. The negative sequence inductance L_{neg} equals $(L''_d + L''_q)/2$. By design, L''_q is not greater than 1.3 L''_d which results in a maximum difference between the machine L_{pos} and L_{neg} of 15 percent. In the case of the Peace River system, this difference is considerably lower. The effect of possible differences between L_{pos} and L_{neg} on the measured equivalent impedance, at most points in the system, will be very small due to other system components for which the positive and negative sequence impedances are identical.

Fourier analysis of the fault current and voltage requires that the power system electric network be linear and time-invariant [11]. Network linearity is affected by saturation in transformers and machines, and time-invariance by protective gap flashovers, line tripouts, and so on. A phase-to-phase fault does not produce overvoltages which would cause significant transformer saturation and as far as machine saturation is concerned, the saturated and unsaturated values of the direct axis subtransient reactance are almost identical. Network time-invariance can be controlled by careful pre-test planning and set-up of the power system test conditions. The machine apparent D and Q-axis impedances change after fault clearance. Provided that the post-fault period included in the analysis is not too long, less than 250 ms say, this change is less than 15 percent - the difference in going from the subtransient to the transient impedances.

2.5 Effect of Fault Duration

The fault duration, and therefore the period of analysis, should be as short as possible. Firstly, during the fault the system generators accelerate causing an increase in the system frequency. The shorter the fault period the smaller the frequency departure from the pre-fault steady state value and therefore the smaller the error in assuming the Thevenin or open circuit voltage to be constant. This is required so that the time-invariance criterion of the impedance measurement technique is satisfied.

Secondly, the subsynchronous content of $V_f(jw)$ and $I_f(jw)$ should be maximized. These are approximately gated 60 Hz cosine waveforms. The frequency spectrum amplitude of such a gated time function is given by:

$$\mathcal{F}\{\cos(w_0 t) \times g(t)\} = \frac{\sin[(w - w_0)\,T/2]}{(w - w_0)} + \frac{\sin[(w + w_0)\,T/2]}{(w + w_0)}$$

$$= \frac{T}{2}\{Sa[(w - w_0)\,T/2] + Sa[w + w_0)\,T/2] \qquad (6)$$

where $g(t) = 1$ for $0<t<T$
$= 0$ elsewhere

where T is the fault duration, Sa[] is the sampling function, and w_0 is the 60 Hz fundamental frequency. This function goes to zero at certain frequencies or nodes as shown in Figure 6. These nodes are undesirable because the system impedance around these frequencies may not be determined accurately. The number of nodes occurring in the subsynchronous region can be minimized by keeping the fault duration small. As indicated in Figure 6, fault duration should consist of an odd number of half-cycles to maximize the subsynchronous spectrum magnitude. This is because the two sampling functions centered around +60 and -60 Hz. interfere with each other constructively for T being an odd number of

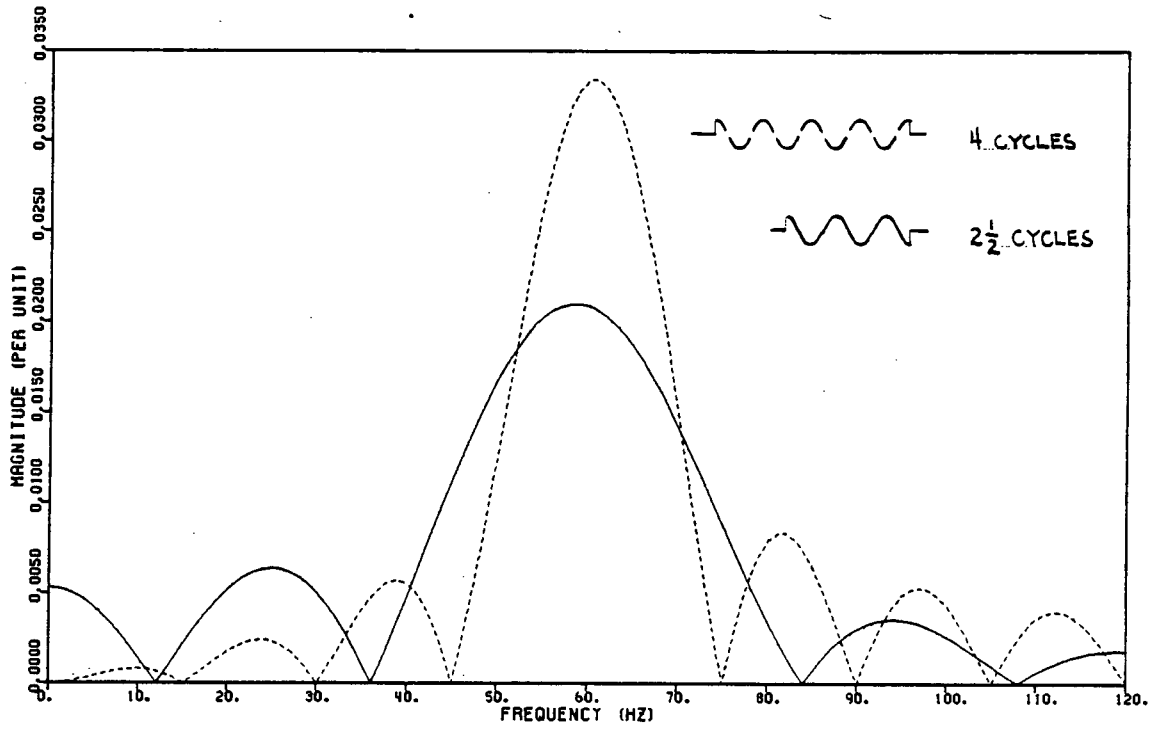

FIGURE 6 - FOURIER TRANSFORM OF A GATED 60 HZ COSINE WAVEFORM

half cycles of w_0 and destructively for T being an even number of half cycles.

3 TEST EXECUTION AND RESULTS

3.1 Test Setup

At the time the impedance measurement test was being developed plans were underway to apply phase-to-phase faults at Williston Substation (at Prince George) as part of acceptance tests for the new Kennedy #3 series capacitor station. With minor modifications, the test setup could also be used for a system impedance test. Williston was not the ideal impedance test location as far as the Hat Creek SSR study was concerned. However, it could provide field test data with which to verify the system computer model and the required test equipment and personnel were already on site. An additional fault to determine the system impedance was therefore scheduled to follow the capacitor test. It was successfully carried out on 1 July, 1981.

A phase A-to-phase B fault was applied at Williston 500 kV substation by isolating a section of bus, applying a bolted fault, and then initiating the fault by closing a circuit breaker. The fault was cleared using the normal bus protection which, unfortunately, did not allow control over the fault duration. Figure 7 shows the essentials of the bus arrangement.

The phase-to-phase voltage appearing across the fault was determined from the phase A and phase B 500 kV capacitive bushing taps on one of the station 500/230 kV auto-transformers. The frequency response of the voltage-measuring circuit was flat from about 5 Hz to well beyond 60 Hz.

The fault current was measured with an existing 500 kV bus protection current transformer (CT). In order to ensure that the core of the CT was not magnetized prior to the test, a variable voltage source was used to desaturate the CT from the secondary side. This was considered advisable

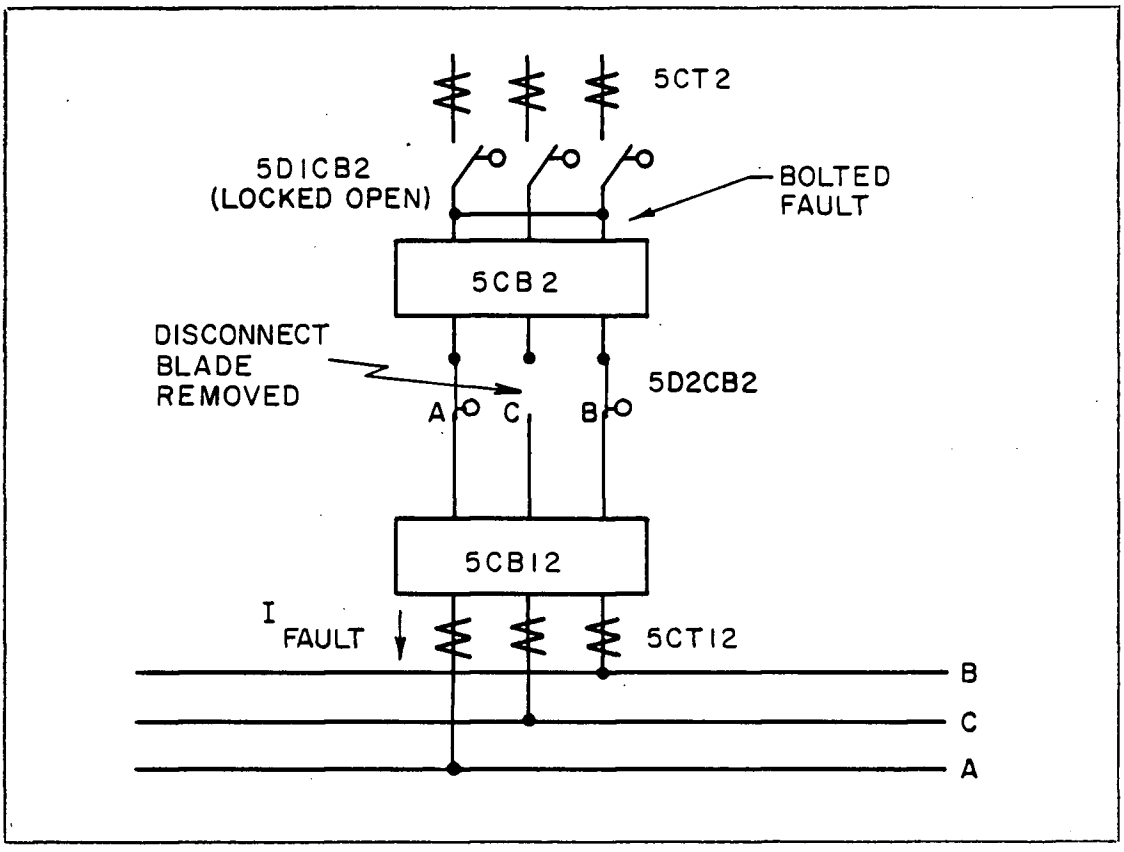

FIGURE 7 - WILLISTON 500 KV BUS FAULT DETAILS

since the bus CT's did not have antiremanence gaps, and other fault tests had taken place earlier on the same day.

All signals were fed into the station control building via shielded control cables, and recorded on an instrumentation tape recorder with a bandwidth of 20 KHz and a resolution of 40 dB. The bandwidth was more than adequate for this application, but the rated resolution of 40 dB (1 part in 100) was relatively poor. The recorded quantities were digitized with a 12 bit analog-to-digital converter at a sampling frequency of 6.6 kHz. A total of 525 milliseconds of each recorded waveform was digitized for computer analysis.

3.2 Recorded Results

The staged fault was of three cycles duration. The only system change that occurred was, as expected, the automatic application of 200 MW of braking resistors at G.M. Shrum, four cycles after fault incidence and their subsequent removal 44 cycles later. This violated the network time-invariance criterion required by the measurement technique. Braking resistor application was anticipated and part of the pre-test planning investigated the effects of these resistors on the frequency scan of the system from the Williston 500 kV bus. As the studies indicated that the frequency scans with and without the brake were virtually identical, it was decided to allow these resistors to function normally and not compromise system stability during the field test. There was also a chance that the test proposal would be rejected if the risk of system instability were to be increased by disabling the braking resistors.

Figure 8 shows the measured voltage appearing across the fault (breaker contacts) and the fault current. CT saturation can affect the accuracy of current measurement. The CT used was rated for a time-to-saturation of one cycle for a fully offset 40 kA rms fault current. Since the measured current was only about 10 kA rms and does not show an appreciable unidirectional offset, it is expected that the CT accurately reproduced the fault current.

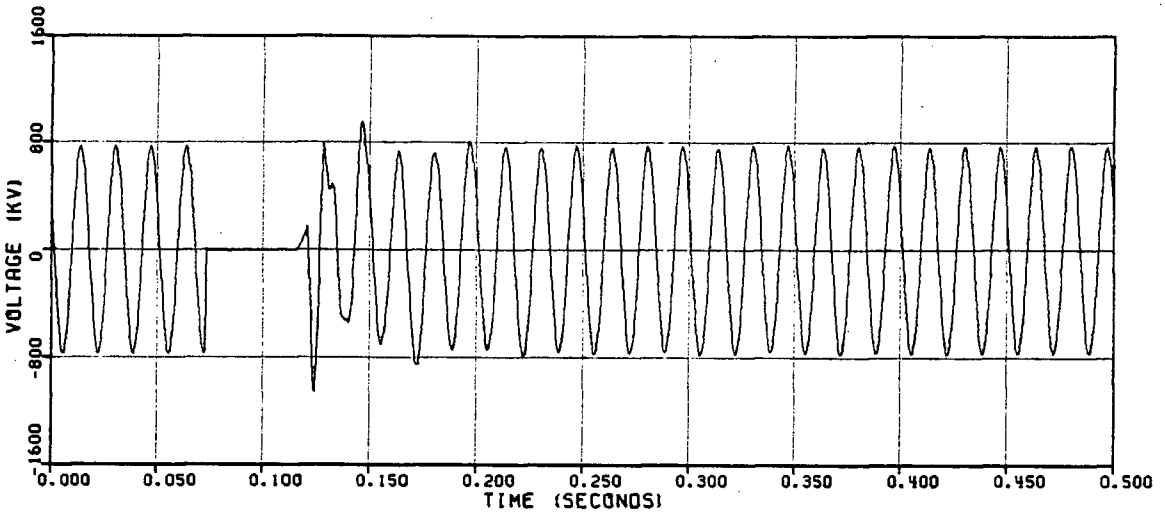

FIGURE 8(A) - MEASURED VOLTAGE ACROSS THE FAULT

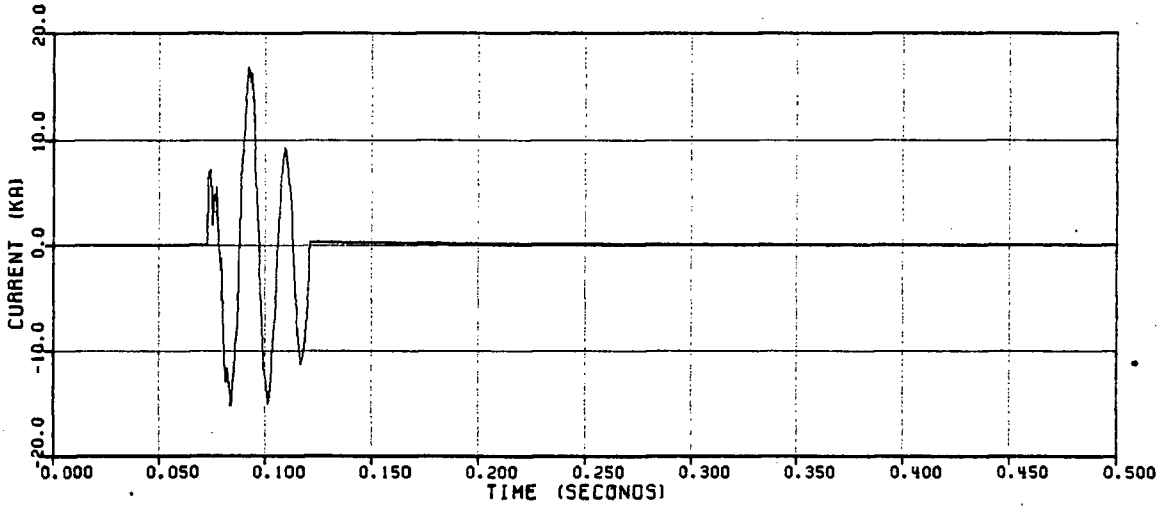

FIGURE 8(B) - MEASURED FAULT CURRENT

4 ANALYSIS OF TEST RESULTS

4.1 Fourier Transform Calculation

The Fourier Transform program used was the one written by Dr. H.W. Dommel as a supporting program for the EMTP. It had the advantage of being interfaced with the EMTP output data format and it uses the classical Fourier Transform formulation and numerical integration. The classical Fourier Transform formulation assumes the time domain signal to be zero outside the time period given (which it would be for this test) and will therefore yield a frequency spectrum down to 0 Hz (DC). Only the non-zero portion of $v_f(t)$ and $i_f(t)$ need therefore be analysed. Details of the Fourier Transform calculation [14] are presented in Appendix II.

4.2 Calculation of Zpos(jw)

The function $v_f(t)$, shown in Figure 9, was created digitally by

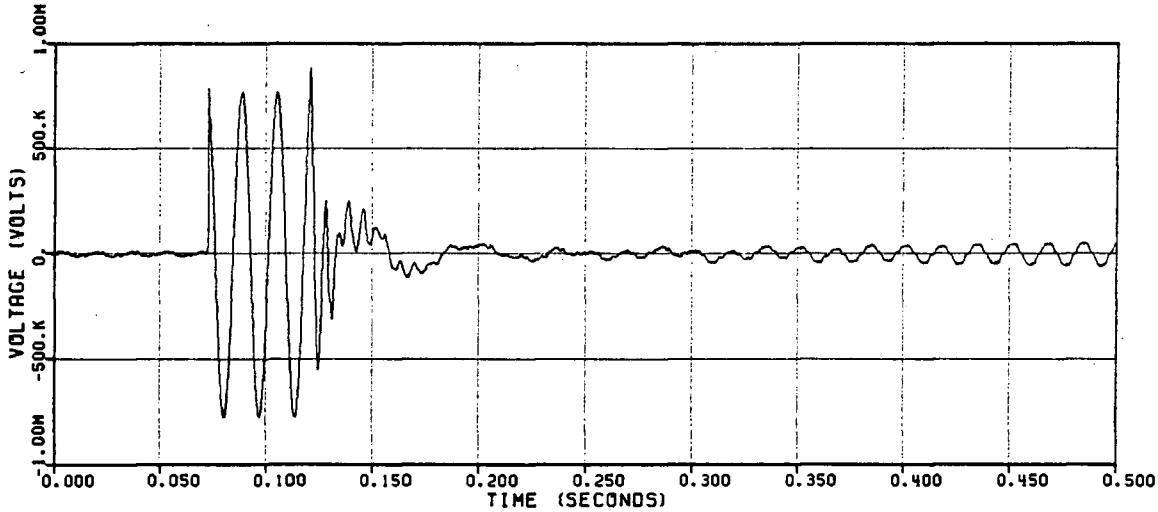

FIGURE 9 - MEASURED FAULT VOLTAGE

extrapolating the measured pre-fault open circuit voltage, $e_{ab}(t)$, into the fault and post-fault time period, and subtracting it from the measured phase-to-phase fault voltage, $v_{ab}(t)$. The exptrapolated $e_{ab}(t)$ did not

perfectly cancel the measured phase-to-phase voltage in the post-fault region. It was expected this was due to the effects of G.M. Shrum braking resistors being applied after the fault, as well as a slight system swing in response to the network disturbance. The voltage response due only to the applied fault, and not to the effects previously mentioned, appears to be completely contained within the first 400 milliseconds. This led to an initial choice of 400 ms as the period for the Fourier analysis.

The Fourier transforms of the fault voltage and current, $v_f(t)$ and $i_f(t)$ are shown in Figures 10 and 11 respectively. The positive sequence

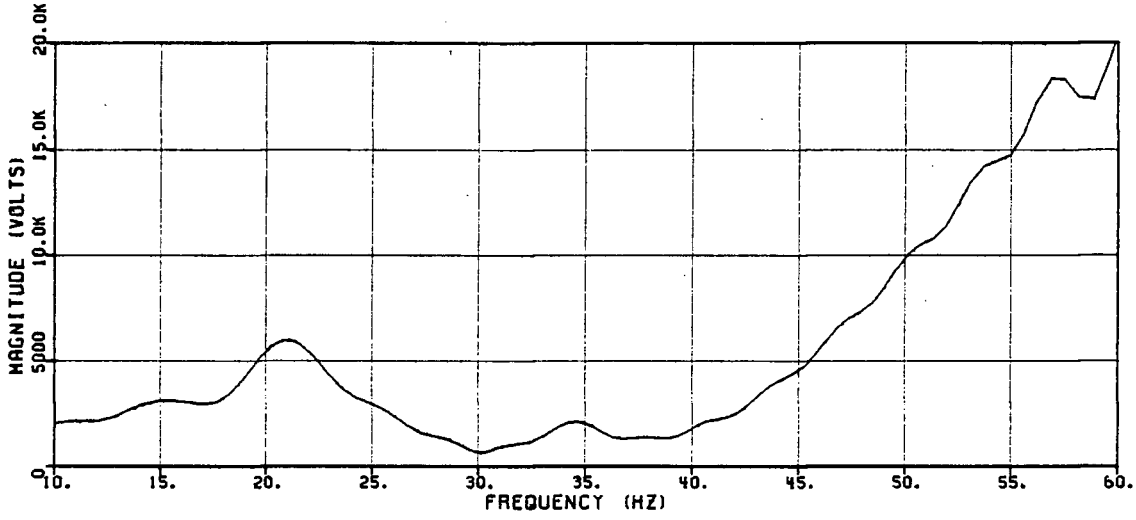

FIGURE 10(A) - FOURIER TRANSFORM OF MEASURED FAULT VOLTAGE (MAGNITUDE)

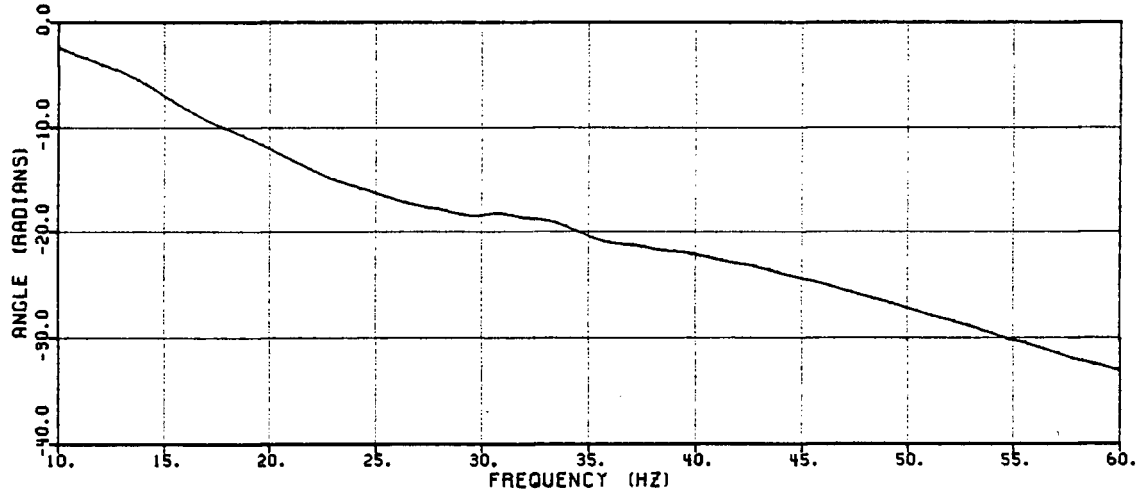

FIGURE 10(B) - FOURIER TRANSFORM OF MEASURED FAULT VOLTAGE (ANGLE)

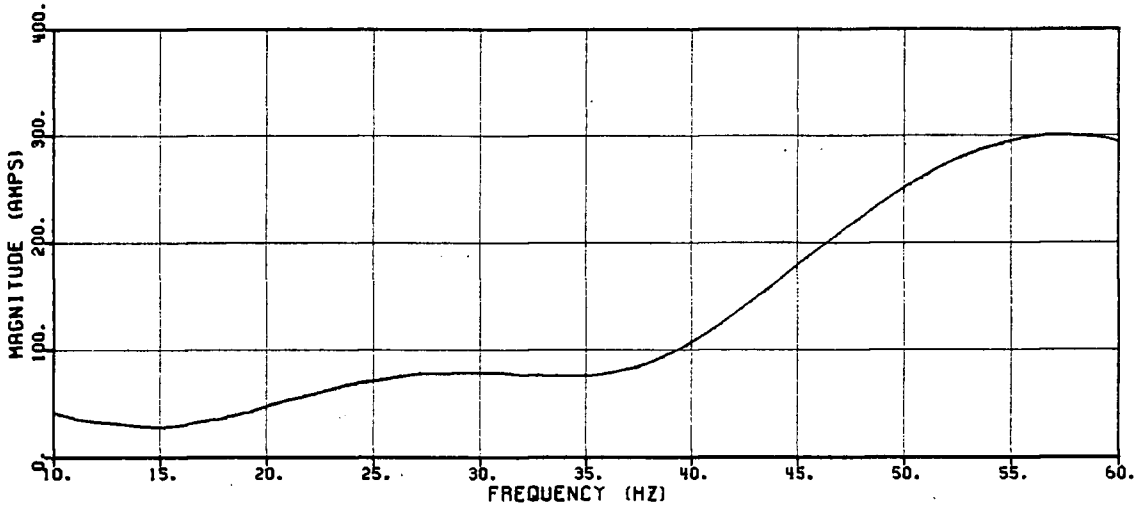

FIGURE 11(A) - FOURIER TRANSFORM OF MEASURED FAULT CURRENT (MAGNITUDE)

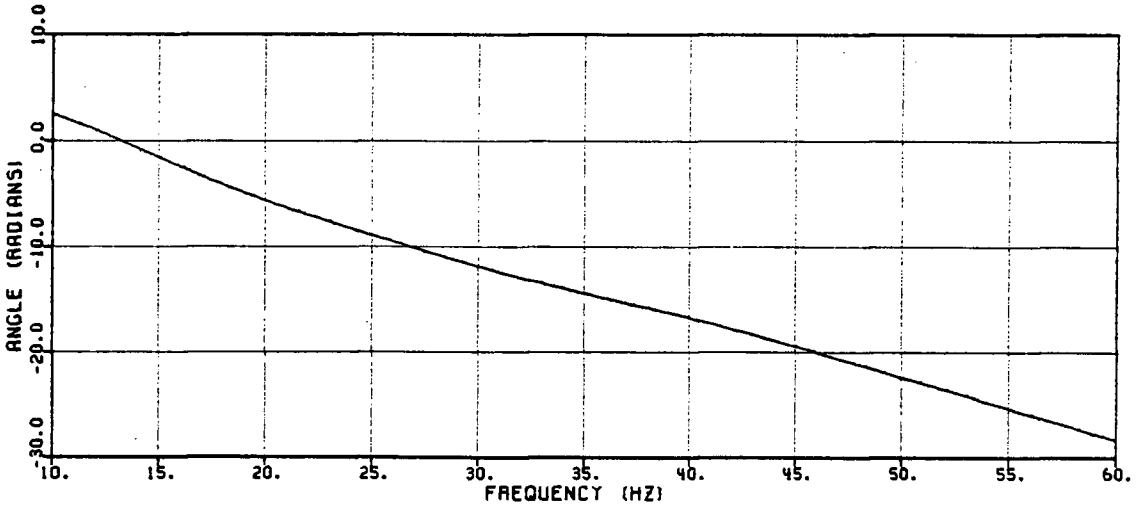

FIGURE 11(B) - FOURIER TRANSFORM OF MEASURED FAULT CURRENT (ANGLE)

equivalent impedance was then formed in accordance with equation (3). The real and imaginary parts of this impedance are shown in Figure 12 for the frequency range of 10 to 60 Hz; the frequency range of interest for subsynchronous resonance studies. Despite the prediction that a fault duration of an even number of half cycles would be less desirable than one of an odd number of half cycles, the three cycle fault produced an adequate current injection in terms of frequency content.

The fault current is zero before and after the fault, requiring no

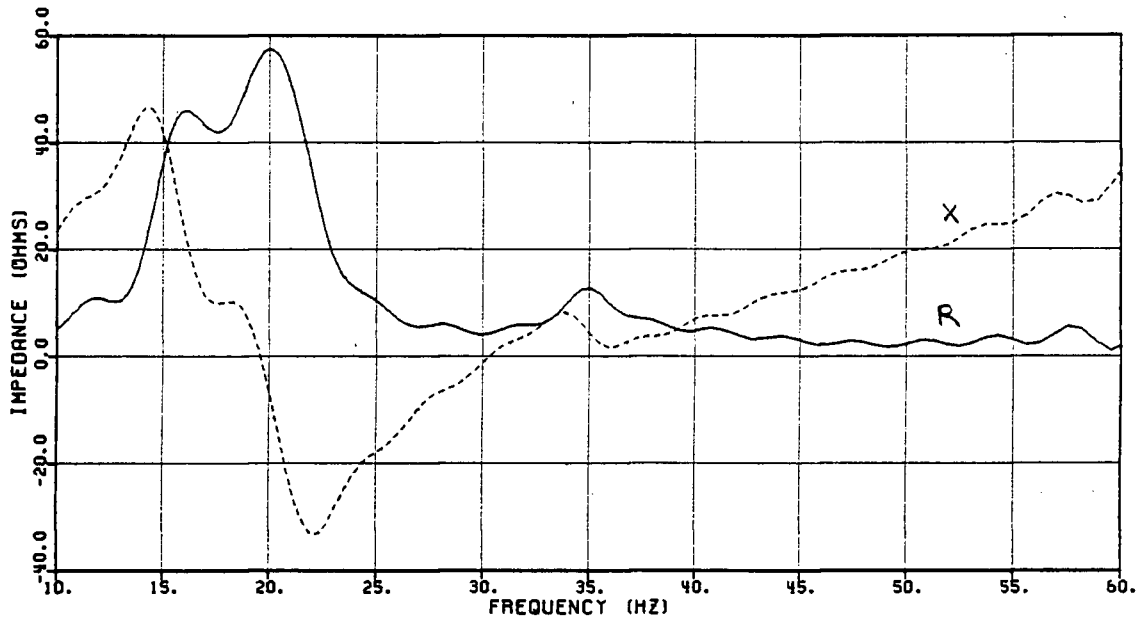

FIGURE 12 - MEASURED SYSTEM EQUIVALENT IMPEDANCE VS. FREQUENCY

truncation for the Fourier analysis but, for the test results presented here, $v_{ab}(t) - e_{ab}(t)$ does not return to zero soon after fault clearance. Amplitude and phase errors [10] result from the truncation of this signal causing the spurious ripples, Gibbs oscillations, observed in the fault voltage spectrum (Figure 10) and the measured system impedance (Figure 12).

Two system resonances, i.e. the frequencies where the equivalent reactance is zero, are evident. The resonance near 30 Hz corresponds to a small equivalent resistance and will be shown to be a series resonance. Similarily, the resonance near 20 Hz, having a large resistance, will be shown to be a parallel resonance.

4.3 Reduction of Gibbs Oscillations

Two methods to reduce the Gibbs oscillation in $v_f(t)$ and $Z_{pos}(jw)$ were tried. Both were successful in the sense that they eliminated the Gibbs oscillation, however neither was desirable in that each appeared to

produce some loss of confidence and detail in the smoothed $Z_{pos}(jw)$.

4.3.1 Analysis of Extended Signal

The first method was simply to extend the period of time being analysed from 400 msec to 2 seconds. This analysis was done using a spectrum analyser operating on the recordings of the impedance test data. Within 40 cycles of the fault application the braking resistors had been removed and within a further 4 cycles the system returned to its initial condition. There was therefore, no fault voltage truncation at t = 2 seconds. Figure 13 shows that the Gibbs oscillation has been eliminated from the system impedance as desired. While there was no apparent way to remove the transient voltage signal

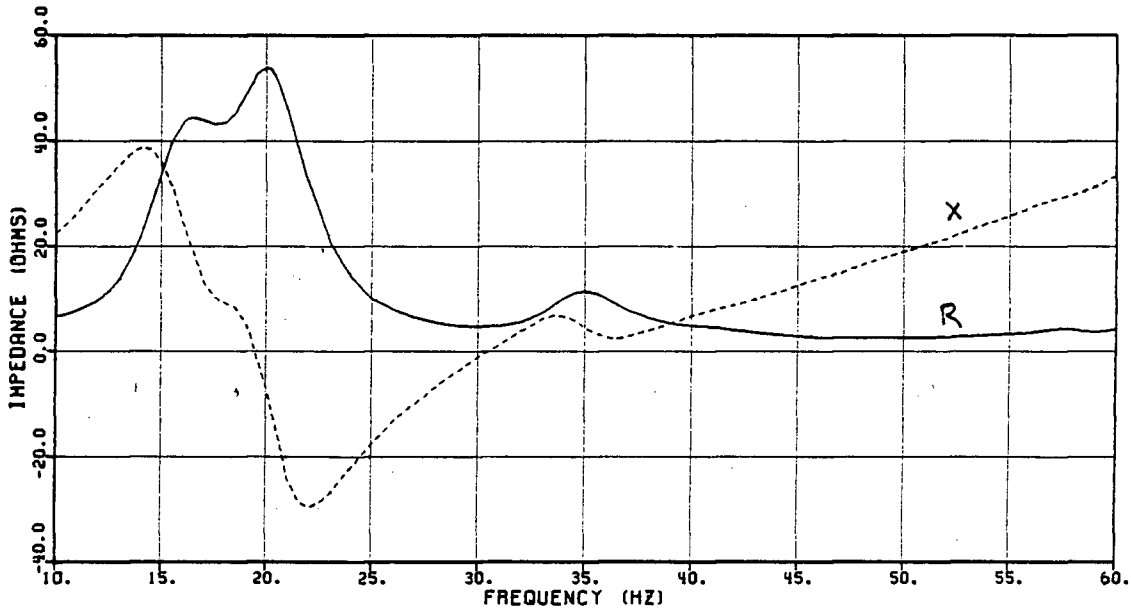

FIGURE 13 - MEASURED SYSTEM IMPEDANCE - REDUCTION OF GIBBS OSCILLATION BY ANALYSIS OF 2 SECOND TIME PERIOD

due to application of the braking resistors, it was questionable whether adding a further external voltage transient, that of the braking resistor clearing, would produce a more accurate $Z_{pos}(jw)$.

4.3.2 Weighting Function (Window)

The second method used to reduce Gibbs oscillations, suggested by Dr. L.M. Wedepohl, was to average $V_f(jw)$ over the period of the Gibbs oscillation. Appendix III shows that this averaging in the frequency domain can be accomplished in the time domain by multiplying the fault voltage by a tapered window function of the form Sa [Pi (t-T/2)/2]. This function is the major lobe of the sampling function centered in the time sample T (Figure 14). It smoothly forces $v_f(t)$ to zero at the beginning and end of the analysis period of T seconds, thereby avoiding truncation and Gibbs oscillations.

Figure 15 shows the new measured Z(jw) calculated using the averaged $V_f(jw)$. Again, the Gibbs oscillations has been eliminated as desired. The new $Z_{pos}(jw)$ is indeed a smoothed version of the old. However, comparing this "averaged" $Z_{pos}(jw)$ with the $Z_{pos}(jw)$ obtained by analysis of the longer duration signals (Figure 13), it appears that the oscillatory characteristic of $Z_{pos}(jw)$ between 15 and 20 Hertz has now been smoothed out. Its existence in Figure 13 would indicate that it is real. Its absence from Figure 15 suggests a loss of data. Use of the averaging technique to smooth out Gibbs oscillations is therefore not advisable here if $Z_{pos}(jw)$ between 15 - 20 Hz. is of interest.

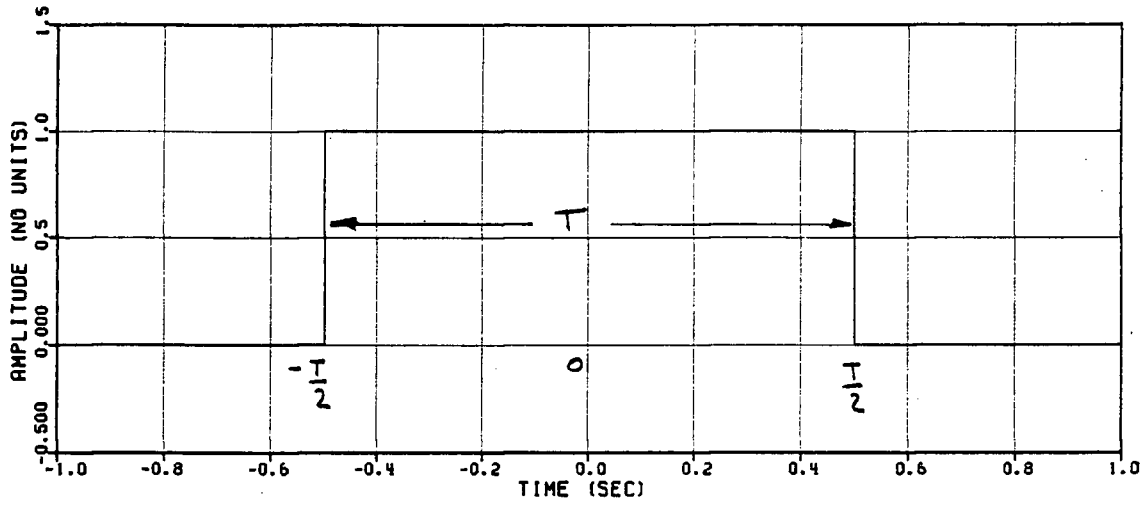

FIGURE 14(A) - GATE FUNCTION

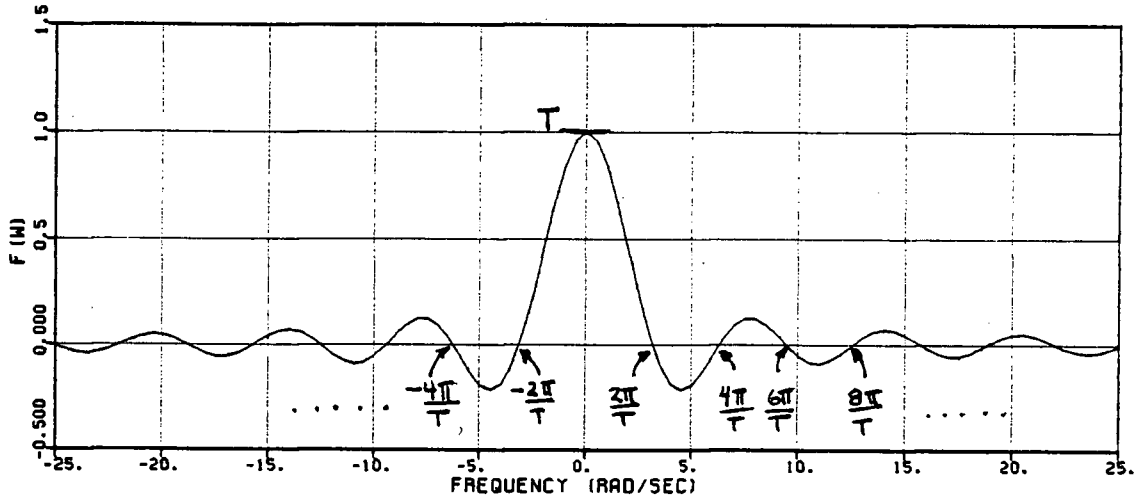

FIGURE 14(B) - SAMPLING FUNCTION

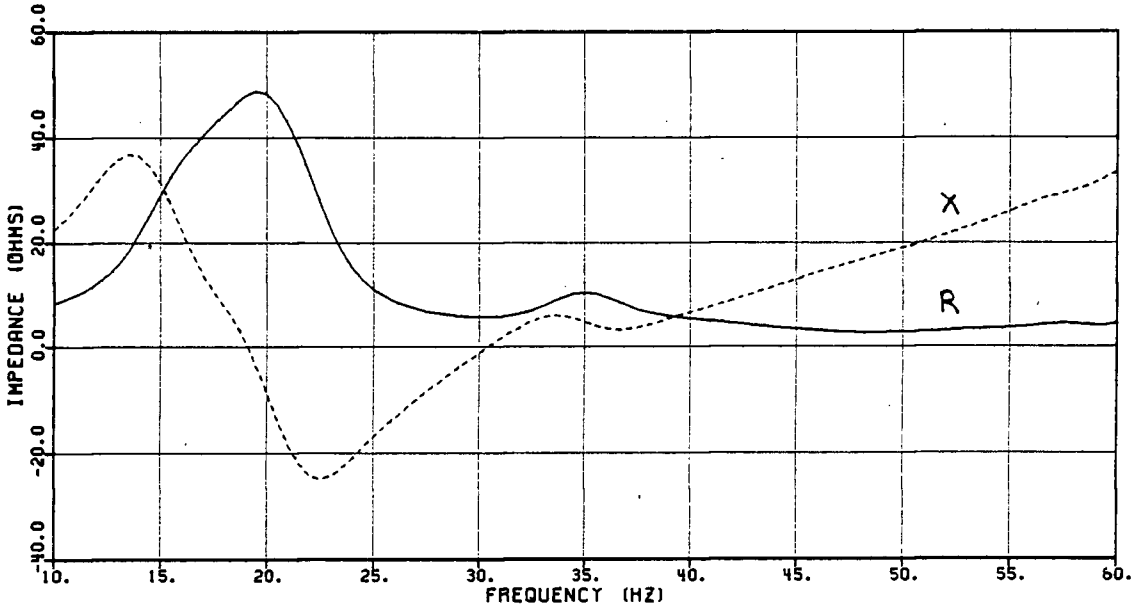

FIGURE 15 - MEASURED SYSTEM IMPEDANCE - REDUCTION OF GIBBS OSCILLATION BY USE OF WINDOWING FUNCTION

5 COMPUTER SIMULATIONS

5.1 500 kV System Model and Simulation Results

With the phase-to-phase staged fault test at Williston Substation having been completed, the known system parameters were used in assembling an EMTP model of the system to represent the field test conditions. The model, shown in the one-line diagram of Figure 16, represents almost all of the B.C. Hydro 500 kV system from the northern hydro plants on the Peace River - G.M. Shrum and Peace Canyon - to the main load centres in the south - Ingledow and Meridian substations. Thus, the same EMTP model could be used for both frequency scan and transients studies.

Transmission lines were modelled by cascaded connections of multiphase pi-circuits, observing proper phasing, transpositions, and physical layout with respect to other EHV circuits on the same right-of-way. The frequency-dependence of the line positive, negative and zero sequence operational impedances was not represented. Line parameters were evaluated at 60 Hz. No transformers were modelled as only the 500 kV transmission was explicitly represented and all generators and loads were represented as equivalents on 500 kV buses. System loads were represented by constant impedance equivalents. All series capacitor banks were represented by lumped capacitance and line reactors by pure shunt reactance.

Hydro plants - six units at G.M. Shrum, two units at Peace Canyon and three units at Mica - were modelled as ideal voltage sources behind source impedances. Machine dynamics were not modelled. The Ra + jX"d of the individual machines with the impedance of their stepup transformers in series were paralleled to produce a source impedance behind each 500 kV

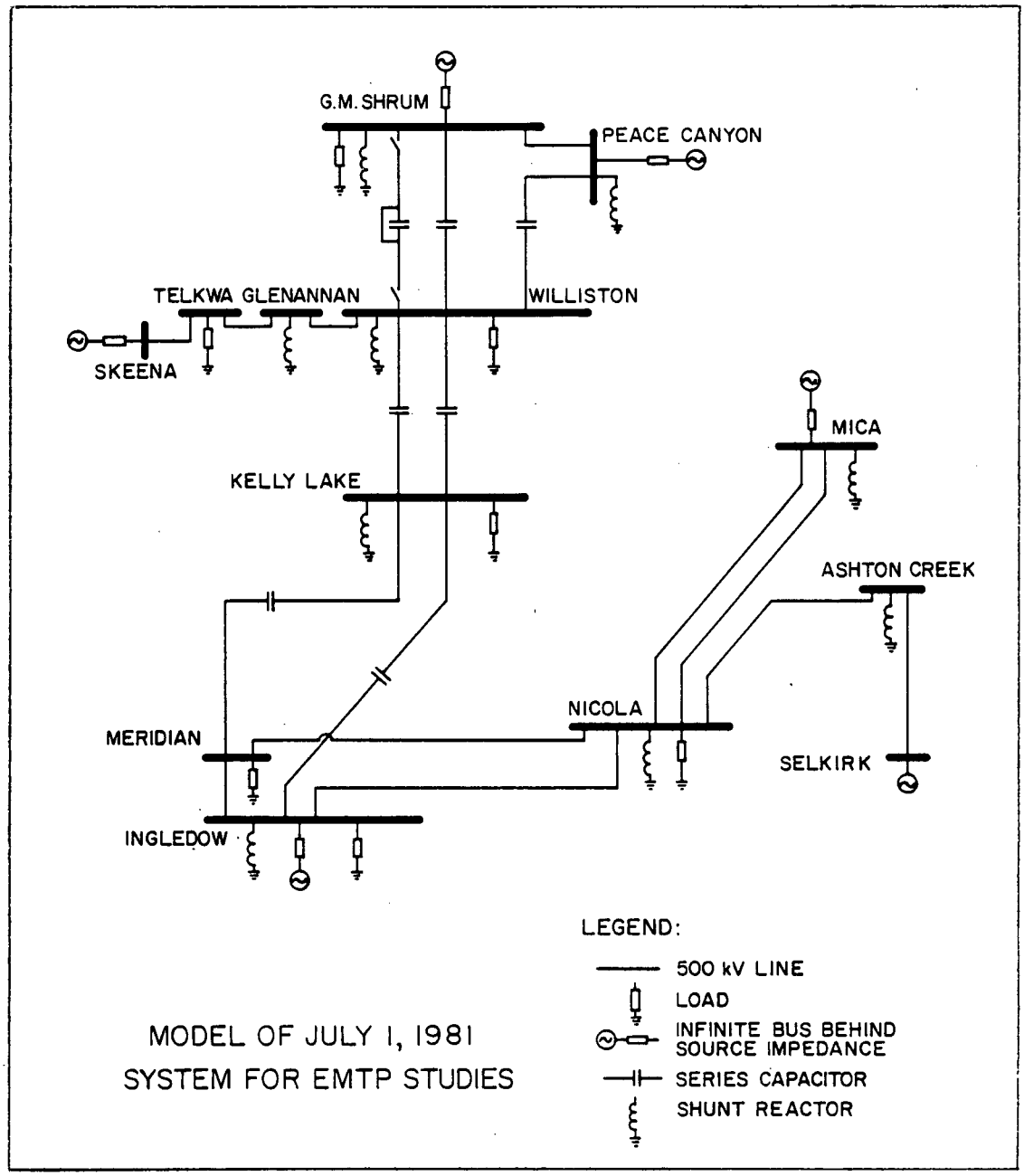

FIGURE 16 - COMPUTER MODEL OF THE B.C. HYDRO MAJOR GENERATION AND 500 KV TRANSMISSION SYSTEM

generation bus.

The tie between Ingledow Substation and the Bonneville Power Administration (BPA) system was represented by an infinite bus behind self and mutual impedances derived from 1-phase and 3-phase fault computations.

Similarly, an ideal source behind a source impedance was placed at Skeena and Selkirk substations.

The results of a system impedance frequency scan from the Williston 500 kV bus, is shown in Figure 17. The calculated system impedance is in

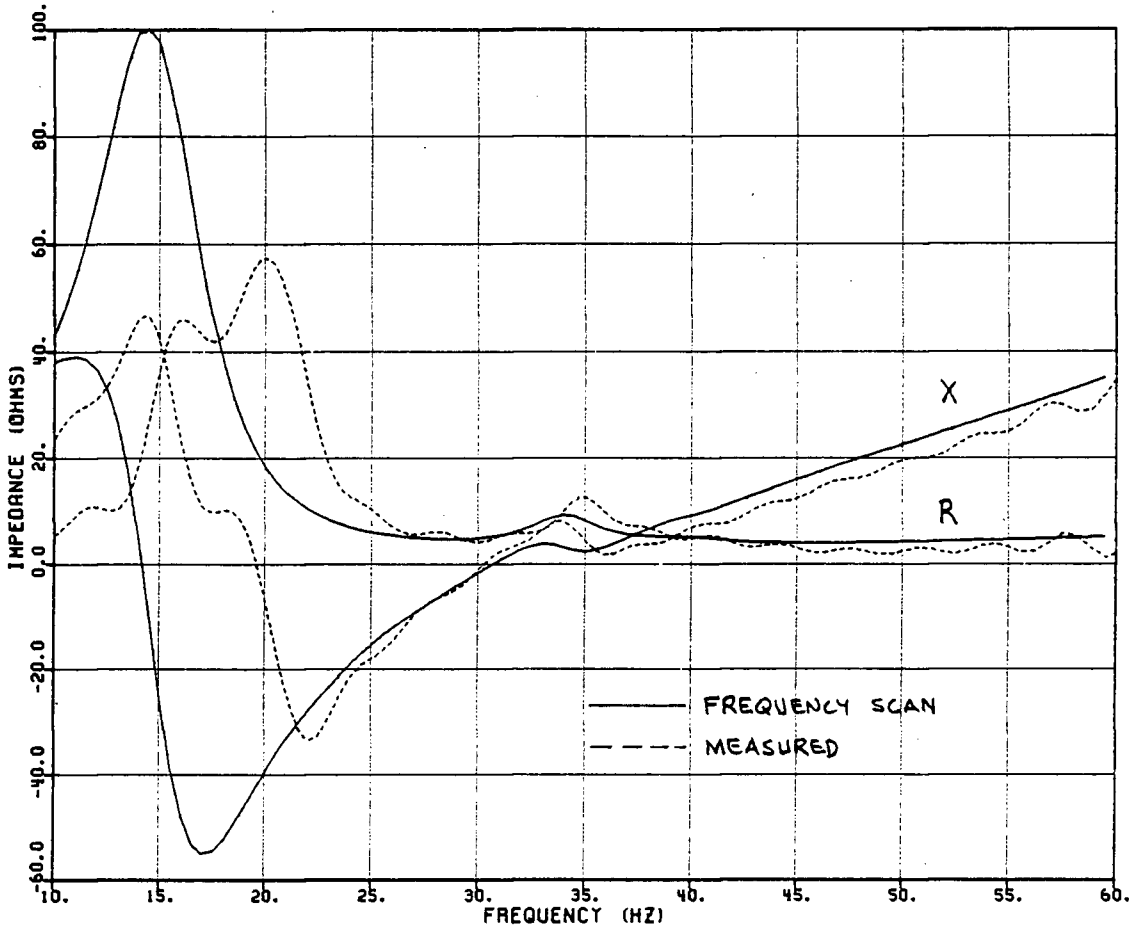

FIGURE 17 - 500 KV SYSTEM MODEL IMPEDANCE FREQUENCY SCAN AND COMPARISON WITH THE MEASURED SYSTEM IMPEDANCE

good agreement with measurement around the system series resonance. They agree to within 0.3 Hz for the series resonance frequence and 4% for the system resistance at series resonance. The model, however, does not give good agreement in the area of system parallel resonance. This discrepancy, combined with EMTP time domain simulations of the test which slightly underestimated the fault current, implied that the system model

was somewhat oversimplified. The model did not explicitly represent any lower voltage transmission or the seven 50 MV.A units at Bridge River. The above model assumed that the effects of the higher impedance paths through the underlying lower voltage transmission would be overwhelmed by the lower impedance 500 kV transmission.

5.2 Extended System Model and Simulation Results

The EMTP 500 kV system model was progressively extended to include some 230 kV and 287 kV transmission as well as the Bridge River generation and its associated transmission. It was not feasible to increase further the complexity of the model because of size limitations imposed by the EMTP. The newly added buses were connected to the 500 kV buses by inductively coupled branches representing the equivalent of one or more actual transformers operating in parallel. Figure 18 shows the final detailed system model, having 112 three-phase nodes.

As more detail was added to the system model the agreement between the frequency scans and the measured system impedance progressively improved. The frequency scan of the final model compared to field results is shown in Figure 19. Although there are still differences in the vicinity of parallel resonance, the shape of the simulated impedance now more closely resembles that of the measured impedance. The impedance in the vicinity of the series resonance is the same as it was for the simpler 500 kV model (Figure 17).

Figure 20 shows the simulated Williston fault current and phase A-to-phase B voltage obtained by using the final detailed system model. Also shown for comparison are the field test measurements.

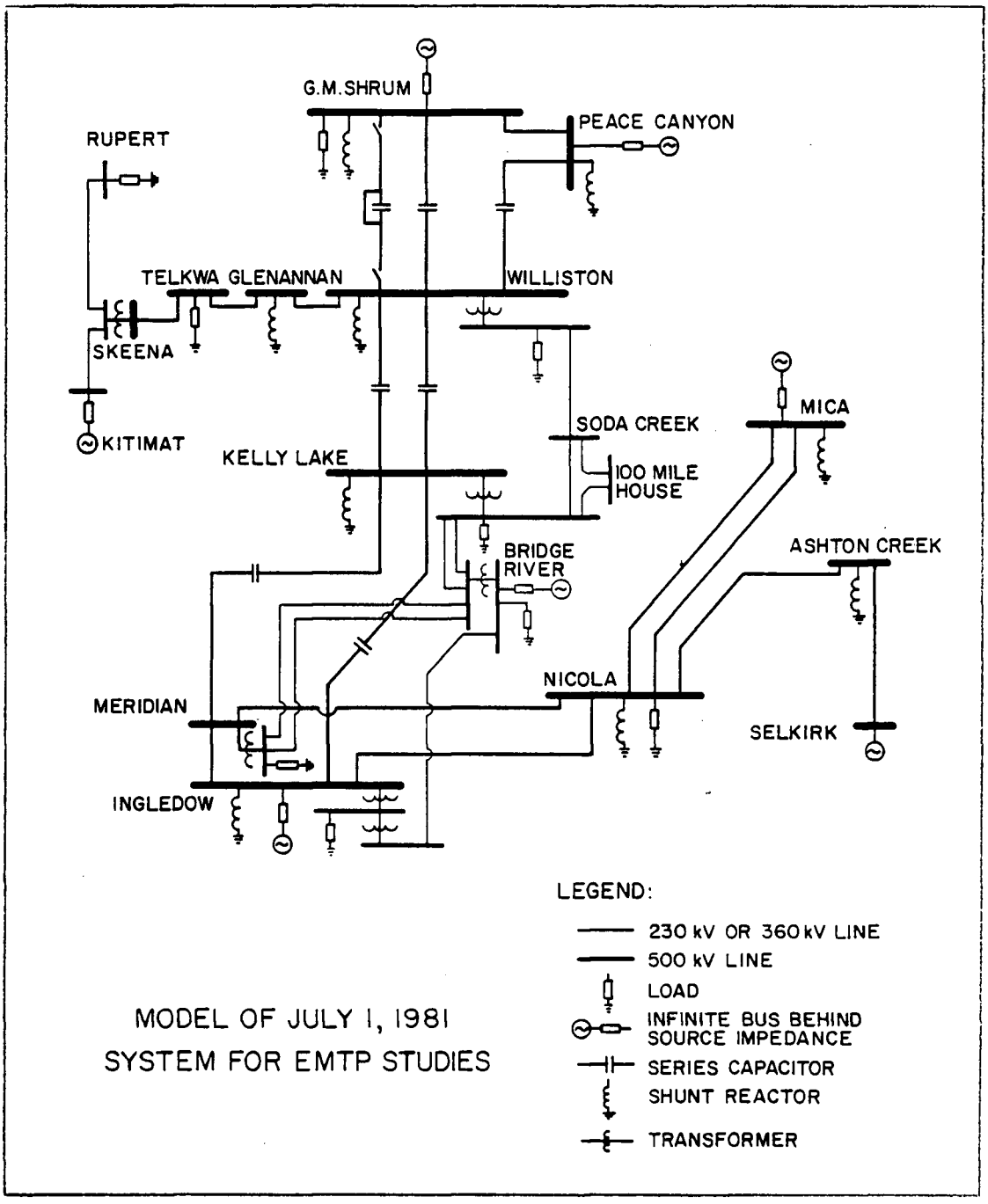

FIGURE 18 - MORE DETAILED SYSTEM MODEL INCLUDING ADDITIONAL NEARBY GENERATION AND SOME 230 KV TRANSMISSION

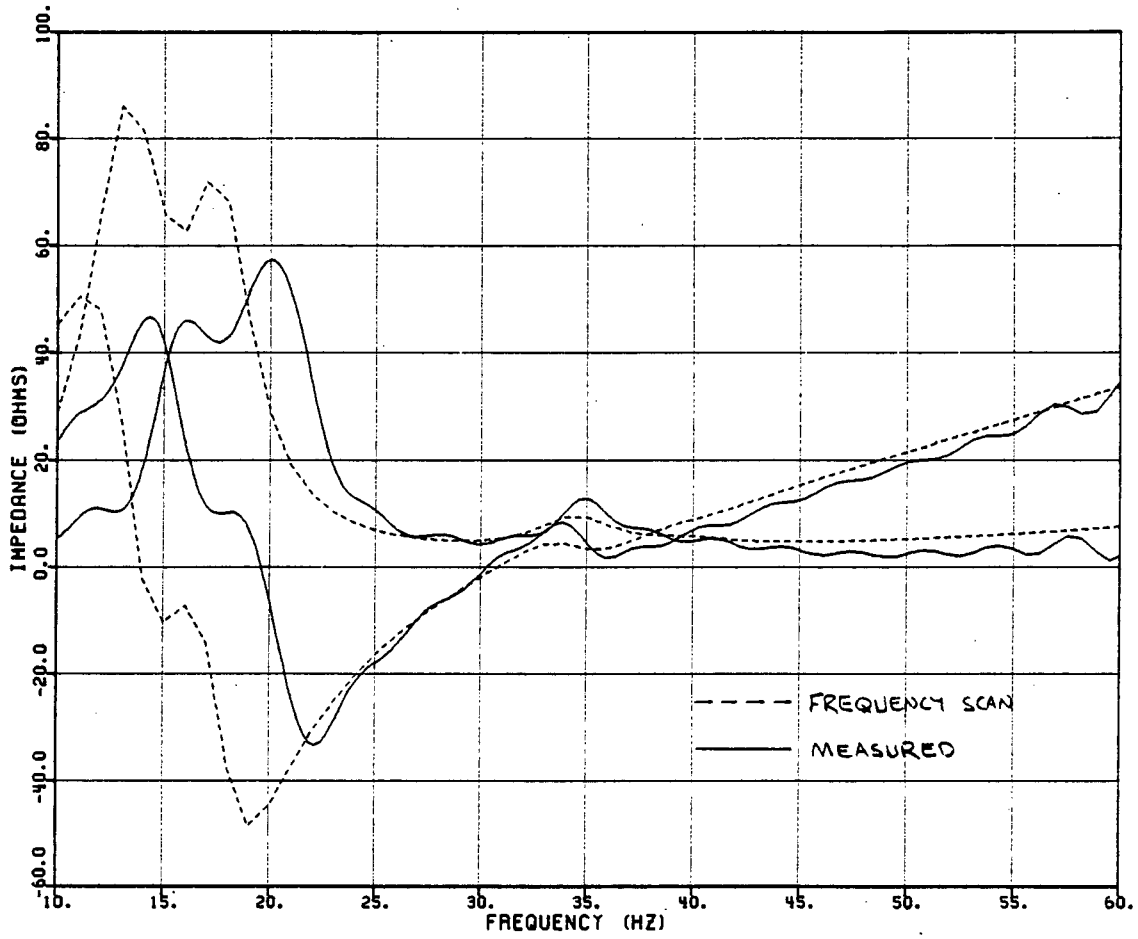

FIGURE 19 - SYSTEM IMPEDANCE FREQUENCY SCAN OF DETAILED EMTP MODEL AND COMPARISON WITH THE MEASURED IMPEDANCE

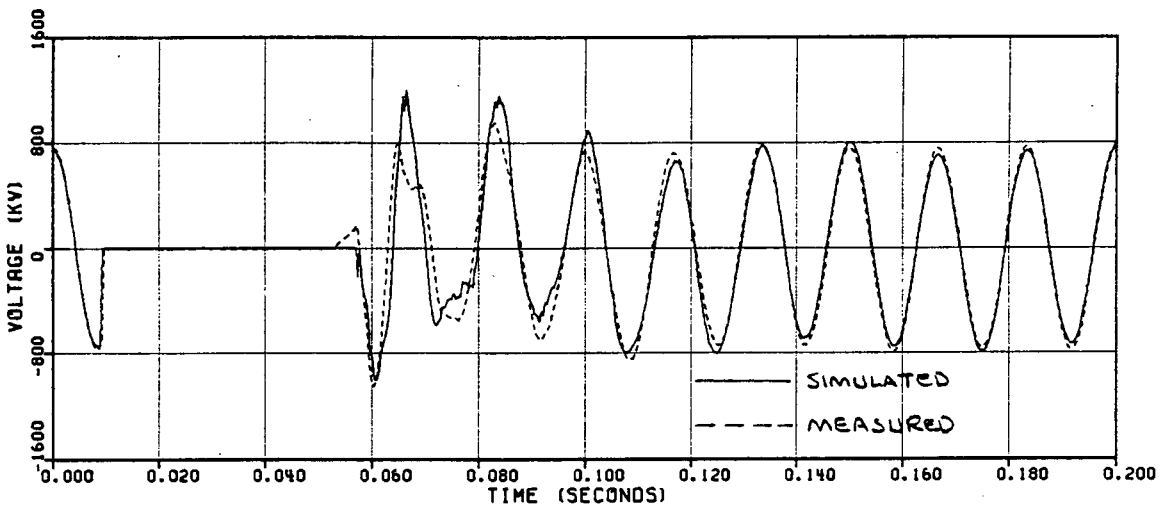

FIGURE 20(A) - COMPARISON OF SIMULATED AND MEASURED PHASE A TO B VOLTAGE

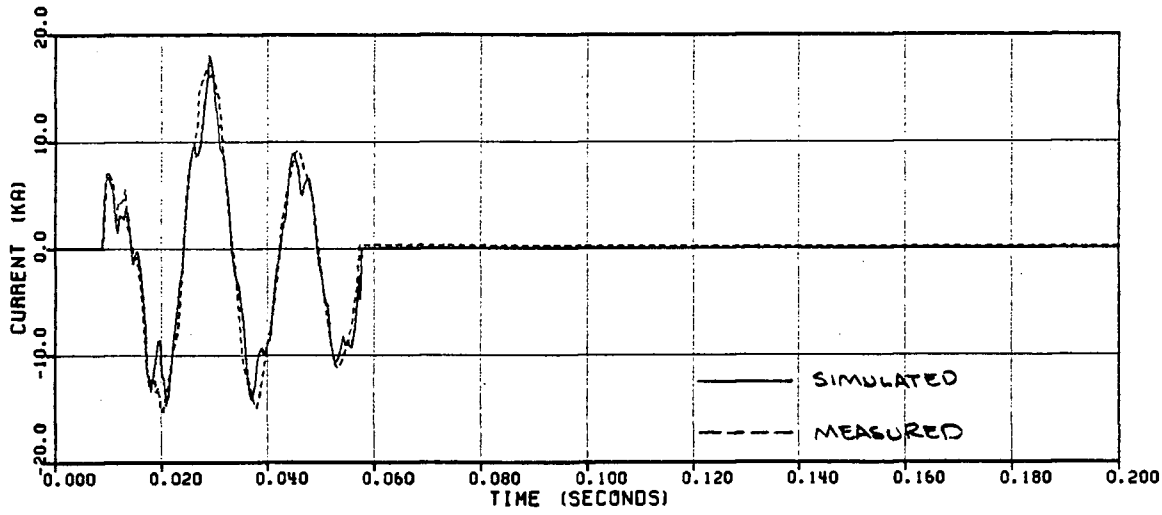

FIGURE 20(B) - COMPARISON OF SIMULATED AND MEASURED FAULT CURRENT

6 EXPLANATION OF DISCREPANCIES BETWEEN MEASURED AND SIMULATED IMPEDANCE

The discrepancy in the impedance between simulation and field test in the area of system parallel resonance and the good agreement elsewhere may be explained. Figure 21 presents a reduced and much simplified system model from Williston where the Nicola, G.M. Shrum, Peace Canyon, Ingledow and Meridian buses are assumed to be short circuits. The series R1, L1, C1 branch basically represents the equivalent for the main series compensated 500 kV transmission circuits out of Williston. The R2, L2 branch is the equivalent for the uncompensated radial 500 kV circuit from Williston to Skeena and the loads along that transmission (modelled in the EMTP), plus the higher impedance underlying subtransmission to the loads out of Williston (not fully modelled). The frequency scan of the simple model [15], also shown in Figure 21, is similar in general shape to the frequency scan of the detailed model. The pole of the impedance function is the parallel resonance between R2, L2 and R1, L1, C1. The zero of the impedance function, at a higher frequency, is the series resonance of R1, L1, C1 and is, for all practical purposes, independent of R2 and L2.

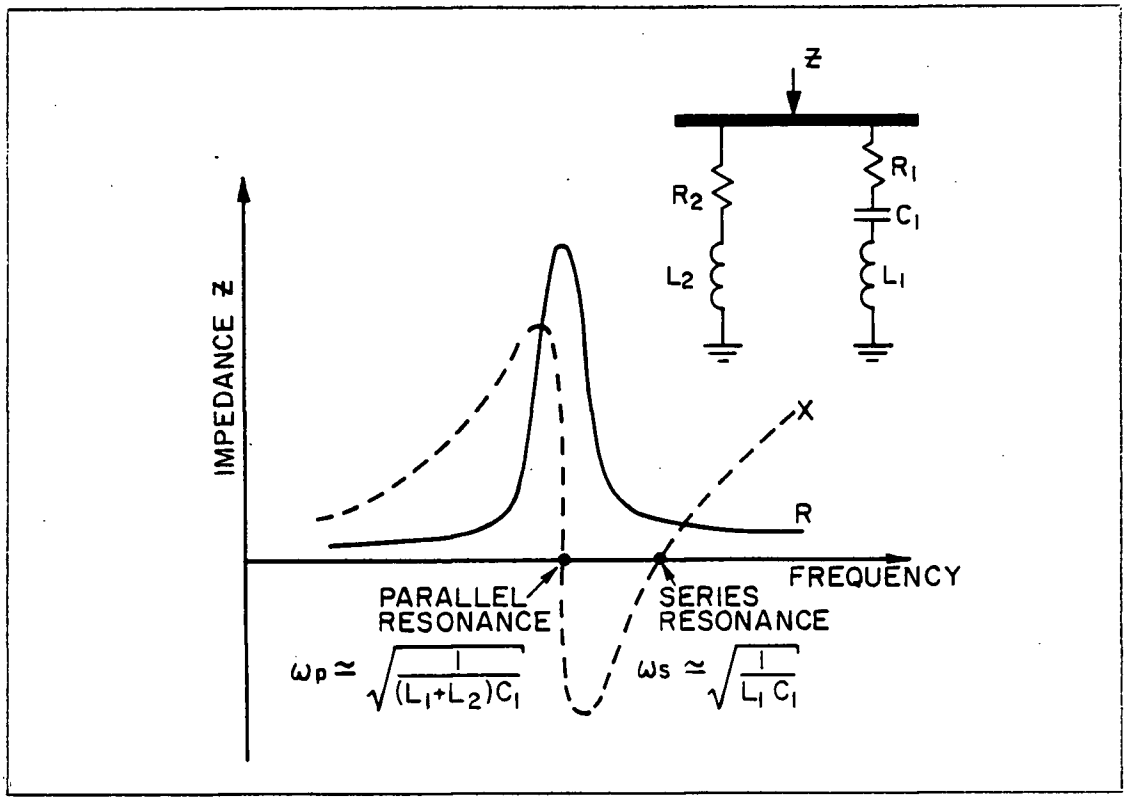

FIGURE 21 - SIMPLIFIED SYSTEM MODEL AND IT'S IMPEDANCE

The system series resonance involves, basically, only the main series compensated transmission, which can be quite accurately modelled in the EMTP - hence the good agreement with the measured $Z_{pos}(jw)$ at the series resonant frequency. Effects which were not accounted for in the simulations are high-gain exciter action, the slight time variance in machine reactances, and saturation. The influence of the combined effects is negligible around the series resonance frequency. The underlying subtransmission and the system loads whose frequency dependence is unknown could not be represented accurately. Both are factors in the behaviour of the system parallel resonance. These shortcomings in the system model account for the discrepancy between simulated and measured $Z_{pos}(jw)$ near the parallel resonant frequency.

7 IMPROVEMENTS TO MEASUREMENT TECHNIQUE

7.1 Computer Simulation Including Lower Voltage Transmission

Dr. Atef Morched of Ontario Hydro subsequently confirmed the above explanations for the discrepancies around the parallel resonance frequency. The author provided Dr. Morched with the test measurements as well as power flow and stability data for the entire B.C. Hydro electrical system down to the substation distribution buses.

The Ontario Hydro study [16] of the test data improved the calculated impedance (as opposed to the measured impedance) by calculating a system impedance frequency scan at the fault location using frequency scaled power flow model data. This was a purely positive sequence model of practically the entire B.C. Hydro transmission system including the lower voltage transmission for which there was not enough room to include in the three phase EMTP model. Also, the simple constant impedance loads of the EMTP model were replaced with static and dynamic loads representations (constant R, L and equivalent machine models) which more correctly accounted for the nature and frequency dependence of the loads. Figure 22 shows that these changes do improve the calculated impedance inasmuch as it now more closely resembles the measured system impedance in the area of the system parallel resonance.

7.2 The Effect of Including System Dynamics

The Ontario Hydro study also improved the measured impedance by improving the system open circuit voltage used to derive the fault voltage. It did so by running a transient stability simulation of the fault application, the fault clearing, and the braking resistor application to determine the way the system equivalence source changed

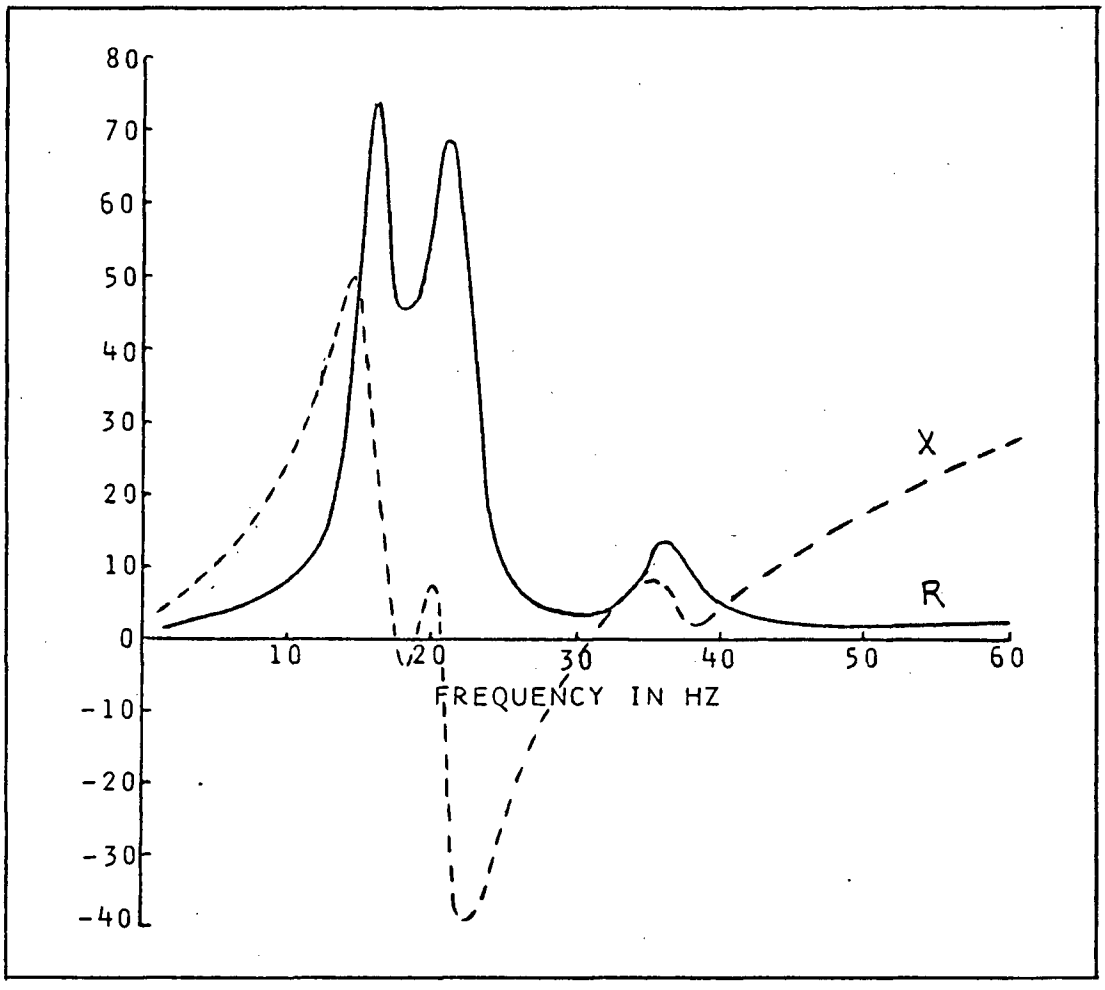

FIGURE 22 - SYSTEM IMPEDANCE FROM EXTENSIVE POSITIVE SEQUENCE SYSTEM MODEL

during the test. This change is shown in terms of it's 60 Hz magnitude (Figure 23) and phase (Figure 24). With the power system dynamics now taken into account, Figure 25 shows the new $e_{ab}(t)$ and Figure 26 shows the resulting $v_f(t)$.

In addition to the above improvement, the Ontario Hydro study calculated the system equivalent positive sequence impedance as:

$$Z(jw) = \frac{1}{2} \frac{G_{vi}(jw)}{G_{ii}(jw)} \qquad (7)$$

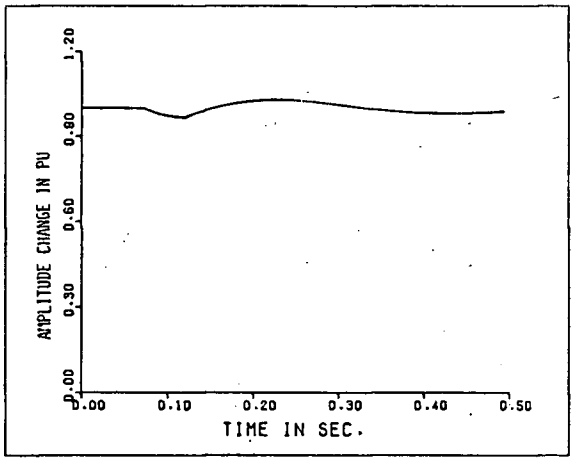

FIGURE 23 - CHANGE IN OPEN CIRCUIT VOLTAGE MAGNITUDE DUE TO SYSTEM IMPEDANCE TEST FAULT

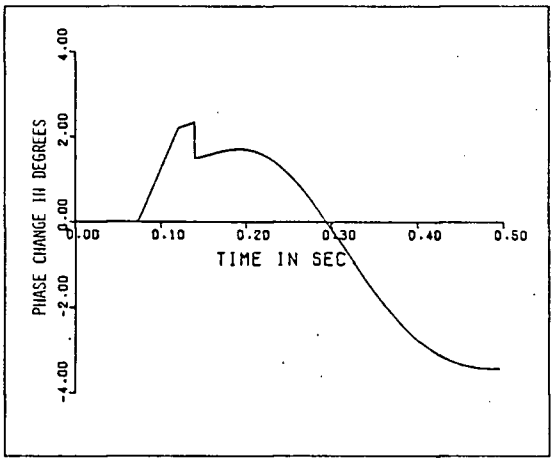

FIGURE 24 - CHANGE IN OPEN CIRCUIT VOLTAGE PHASE DUE TO SYSTEM IMPEDANCE TEST FAULT

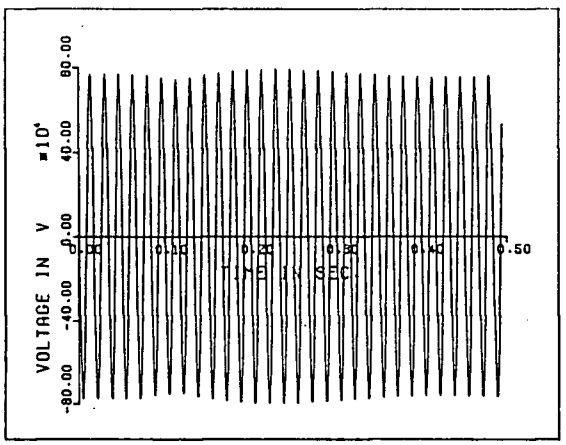

FIGURE 25 - OPEN CIRCUIT VOLTAGE CORRECTED FOR SYSTEM DYNAMIC SWING

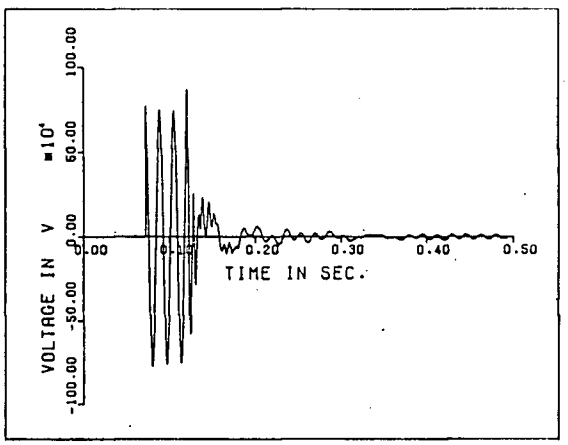

FIGURE 26 - FAULT VOLTAGE CORRECTED FOR SYSTEM DYNAMIC SWING

where $G_{ii}(jw)$ is the auto power spectrum of the current and $G_{vi}(t)$ is the cross power spectrum between the voltage and the current [7,8,14]. This technique reduces the effect of deterministic errors introduced by the measurements as well as random errors. The newly derived, measured system impedance is shown in Figure 27. The correspondence between the Ontario Hydro study's calculated and measured impedance is very good throughout the entire subsynchronous frequency range. It represents a definite improvement over the results initially obtained, especially in the area of

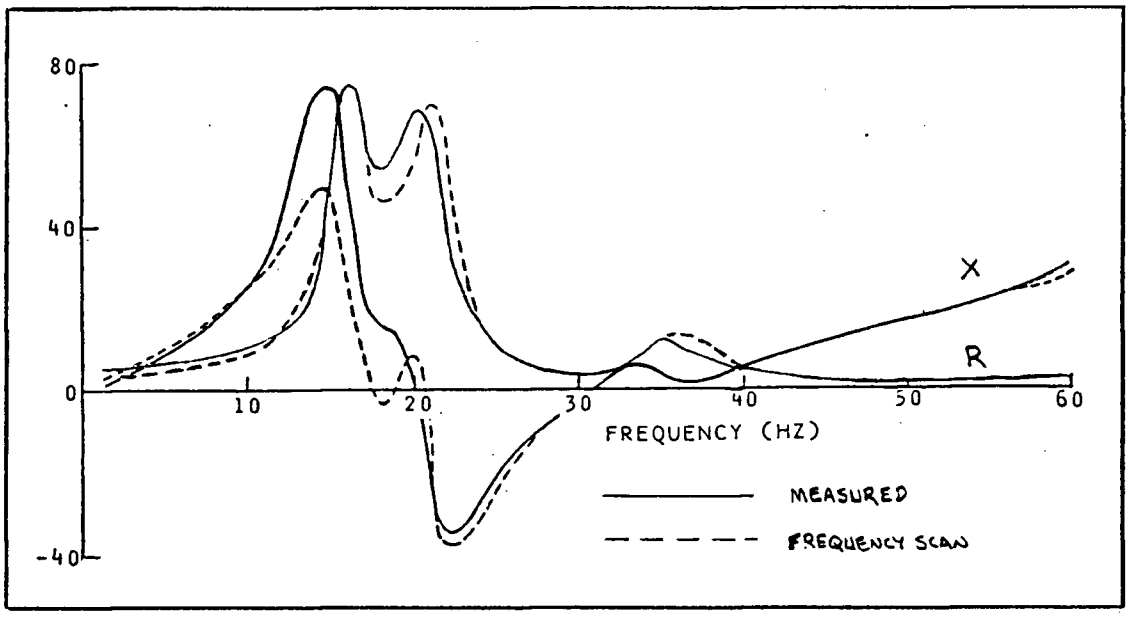

FIGURE 27 - MEASURED SYSTEM IMPEDANCE CORRECTED FOR SYSTEM DYNAMIC SWING COMPARED WITH THE SYSTEM IMPEDANCE FREQUENCY SCAN OF THE EXTENSIVE POSITIVE SEQUENCE MODEL

the system parallel resonance.

In order to see the contribution made by each of the improvements, $Z_{pos}(jw)$ was recalculated using the above auto- and cross-correlation formula acting on the $v_f(t)$ signal derived using the original (unimproved) $e_{ab}(t)$. The resulting $Z_{pos}(jw)$ was identical to the one derived without using correlation (Figure 12). It is therefore concluded that the improvement Ontatio Hydro achieved in their calculation of the measured $Z_{pos}(jw)$ is essentially entirely due to his inclusion of the system dynamic swings in $e_{ab}(t)$. Correlation did not help here because (1) there was an adequate signal-to-noise ratio to begin with and (2) the duration of the signal of 400 msec was not long enough to allow the cross-correlation to reject any voltage signal not due to the fault current signal, such as the system dynamic swing and the voltage transient due to the braking resistor application. Correlation does help in the

interpretation of the system impedance in that the cross and auto power spectrums can be used to provide an estimate of the signal-to-noise level of $Z_{pos}(jw)$ and the confidence interval associated with the measured impedance at each frequency.

7.3 Supersynchronous Impedance and Minimum Required Current

While the main purpose of this test was to measure the system's subsynchronous equivalent impedance, the measurement technique is equally valid at supersynchronous frequencies. This data was also of interest in that comparison of the measured and calculated $Z_{pos}(jw)$ could help determine the upper frequency limit for which the EMTP system model was valid. Figure 28 shows the frequency spectrums $V_f(jw)$, $I_f(jw)$, and the measured and calculated $Z_{pos}(jw)$ to 200 Hz.

Two characteristics of the measured impedance are apparent. The first characteristic is a noticable change in slope in the reactance curve above 60 Hz. This may be due to induction machine effects from motor loads in the vicinity of the measurement point. Loads in the EMTP model were simplistically represented by resistors which would explain why the calculated impedance does not exhibit this behaviour. The second and more limiting characteristic of the measured impedance is it's instability in the vicinity of the $I_f(jw)$ nodes at 80 and 100 Hz. and the poor correlation between the measured and calculated impedance above 100 Hz. These are problems of an insufficient level of current injection which was identified earlier as being a limitation of this measurement technique. Refering to Figure 28 then, a minimum value of current injection of about 20 Amps is apparently required to determine the system impedance. It is expected that with higher resolution recordings of the field data, the minimum current injection required would decrease and the highest

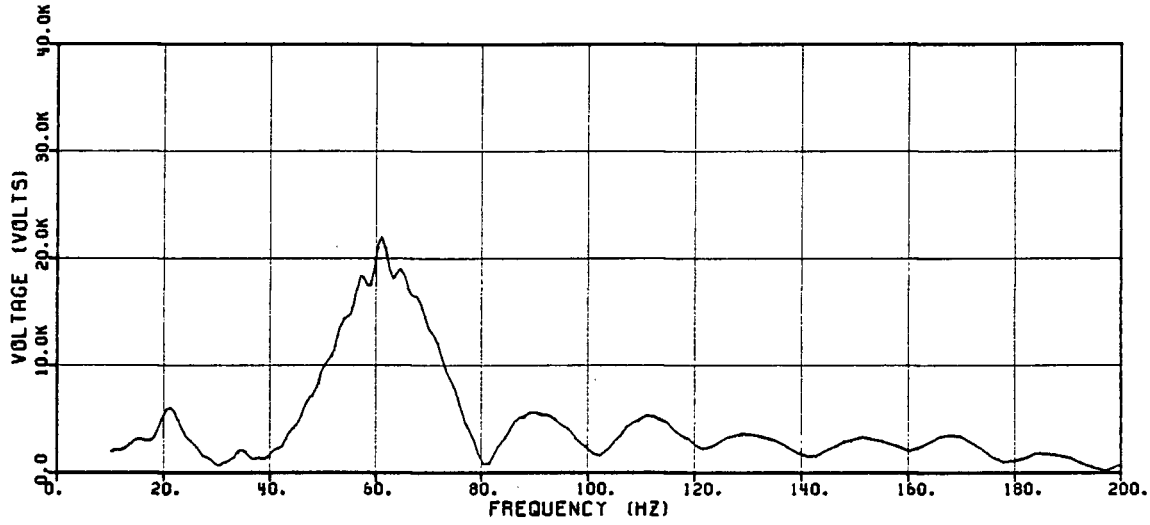

FIGURE 28(A) - FREQUENCY SPECTRUM OF FAULT VOLTAGE (MAGNITUDE ONLY)

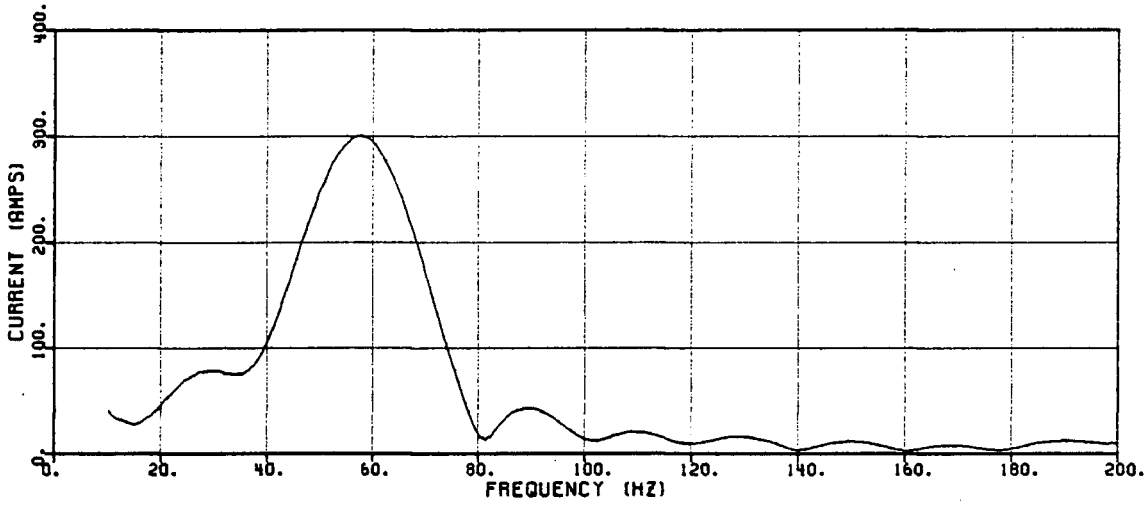

FIGURE 28(B) - FREQUENCY SPECTRUM OF FAULT CURRENT (MAGNITUDE ONLY)

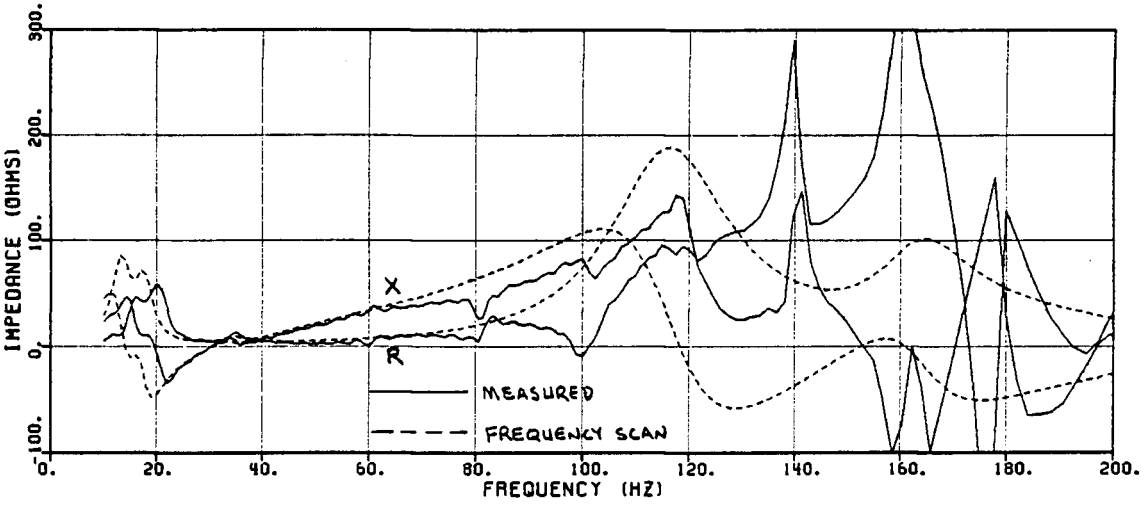

FIGURE 28(C) - MEASURED AND CALCULATED SYSTEM IMPEDANCE

frequency at which the system impedance could determined would increase.

Since reasonable measurements of the system impedance were obtained for current injections as low as 20 Amps, the digitized fault current must be reasonably accurate to at least this resolution. The resolution of the tape recorder, for the impedance test, must therefore have been at least 20 Amps in 20,000 (the peak signal value), or 60 dB which is much greater than its 40 dB rating. It is possible that the limiting factor was not the resolution of the tape recording but instead the resolution of the 12 bit analog-to-digital converter, which was 1 part in 4096 or 72 dB.

The current injection levels obtained at frequencies close to the system parallel resonance (15-20 Hz) are above the minimum acceptable level. The discrepancies between the measured and calculated system impedance at these frequencies are therefore more likely due to the EMTP system model deficiencies previously discussed than to measurement inaccuracy.

A recent Ontario Hydro test [17] demonstrated the value of high resolution recordings. System impedance tests were done on the Ontario Hydro distribution system using the application and removal of shunt capacitors as the system disturbance. For this test the "fault" voltage was derived in real-time by removing the 60 Hz steady state voltage from the system node voltage before recording it. The instrumentation scaling could then be done on the transient voltage rather than on the larger steady state voltage thereby making better use of the resolution of the recording device. A 14-bit resolution digital storage oscilloscope was used to digitize the data directly - ie: there was no intermediate tape recording. This improved resolution allowed good impedance measurements up to 5 KHz. The problem of low signal levels at the $I_f(jw)$ nodes was solved by repeating the test a number of times with different fault

durations and averaging the impedance spectrums obtained. Since it is unlikely that any two tests would have $I_f(jw)$ nodes at the same frequency, this averaging tended to eliminate (dilute) the numerical instability associated with these nodes.

Another important aspect of Ontario Hydro's test was the use of a capacitor as a disturbing element. The capacitor's impedance at low frequencies, particularily the 60 Hz system frequency, is high making it equivalent to a relatively mild system fault. However, at higher frequencies the capacitor's impedance is low. This frequency dependent fault impedance will therefore tend to accentuate the high frequency content of the transient current relative to its low frequency content, making it better suited to a supersynchronous impedance test than a zero impedance bolted fault would be. The capacitor application has only a small effect on the reactive power flow and practically no effect on the system real power flow. The system open circuit voltage is almost certain to be unaffected by this type of system disturbance and is therefore likely to remain constant. This would eliminate the fault voltage signal truncation and the resulting Gibbs oscillation problems that arose in the B.C. Hydro test.

7.4 Modal (Sequence) Analysis of Test Results

It was previously stated that the type of fault chosen for the impedance tests would have to provide only positive sequence excitation, at subsynchronous frequencies, to the system. Section 2.2 showed that a phase-to-phase fault would do this, with certain assumptions, and rejected all other types of faults because they also provided some zero sequence excitation and response that could not be separated from the desired positive sequence quantities. Mr. J.H. Sawada of B.C. Hydro has now

extended the usefulness of the impedance measurement technique by applying the symmetrical component transformation (as a special modal transformation), in the time or the frequence domain, to the fault voltages and currents measured for all three phases and obtains the sequence impedances as [18]:

$$\begin{aligned} Z_0(jw) &= V_{f0}(jw)/I_{f0}(jw) \\ Z_1(jw) &= V_{f1}(jw)/I_{f1}(jw) \\ Z_2(jw) &= V_{f2}(jw)/I_{f2}(jw) \end{aligned} \qquad (8)$$

The above equations once again assume a balanced impedance matrix. The more general three phase impedance matrix [Z(jw)] can be derived using the matrix equation:

$$\begin{bmatrix} Z_{aa} & Z_{ab} & Z_{ac} \\ Z_{ba} & Z_{bb} & Z_{bc} \\ Z_{ca} & Z_{cb} & Z_{cc} \end{bmatrix} = \begin{bmatrix} V_{a1} & V_{a2} & V_{a3} \\ V_{b1} & V_{b2} & V_{b3} \\ V_{c1} & V_{c2} & V_{c3} \end{bmatrix} \begin{bmatrix} I_{a1} & I_{a2} & I_{a3} \\ I_{b1} & I_{b2} & I_{b3} \\ I_{c1} & I_{c2} & I_{c3} \end{bmatrix}^{-1} \qquad (9)$$

where all quantities are functions of frequency and the above equation holds at each frequency, and where the numerical subscripts for the voltages and currents refer to data from different tests done with the same system conditions. For example, tests 1, 2 and 3 could be three separate line-to-ground fault tests on phases a, b and c respectively.

Such actual knowledge of [Z] as a function of frequency would be invaluable in creating power system frequency dependent equivalents [19,20]. These would save having to model, explicitly, large parts of the power systems in order to represent their frequency dependent characteristic.

8 CONCLUSIONS

This thesis describes a technique, and presents field test results, for measuring the subsynchronous positive sequence equivalent impedance, as a function of frequency, of an operating power system using Fourier analysis of the fault current and phase-to-phase voltage obtained from a staged phase-to-phase fault. As no external source of excitation is required, coupling problems are eliminated. The good correlation between EMTP simulation and the field test results justify the approximations of network linearity, time invariance, and equality between the positive and negative sequence equivalent impedances, which are required by the technique.

The EMTP, using a model of the present B.C. Hydro high voltage (500 kV) system, is able to determine the equivalent network subsynchronous impedance in relation to frequency in good agreement with field measurements, except in the vicinity of system parallel resonance. This model provided the system series resonance within 0.3 Hz and equivalent resistance within 4 % of the measurement value, making it sufficiently detailed for use in Hat Creek SSR studies.

Reasons for the discrepancy between the measured and calculated system parallel resonance impedance were given and subsequently confirmed by the work done at Ontario Hydro. Since SSR is not likely to occur at a system parallel resonance, the very detailed modelling required to correctly model the parallel resonance behaviour was not considered necessary. If, for some other application, the system parallel resonance is of interest, the system model must be expanded to include more of the lower voltage transmission and perhaps frequency dependent equivalents of the local system loads.

Two methods for eliminating the Gibbs oscillations from the measured fault voltage and system impedance were tried. Both were successful but they reduced confidence in the resulting system impedance and were therefore not

used. Using a system disturbance less severe than a bolted fault should leave the system open circuit voltage constant and eliminate the fault voltage truncation that caused the Gibbs oscillations.

While it was primarily the system subsynchronous impedance that was of interest, the impedance test is equally valid at supersynchronous frequencies and has been successfully applied by others at frequencies up to 5 kHz. It was also noted that a phase-to-phase fault was used in this test so that directly measurable voltage and current quantities could be used to determine the system positive sequence impedance. The analysis technique has also been extended by others to a modal (eg: symmetrical components) transformation prior to the spectral analysis so that, provided there is enough current injection, any modal impedance can be derived from the same modal fault voltage and current.

With the validity of the computer model of the present B.C. Hydro system established, EMTP impedance frequency scans of future transmission networks can therefore be used with confidence in SSR investigations.

9 REFERENCES

[1] M.C. Hall,"Experience with 500 kV Subsynchronous Resonance and Resulting Turbine Generator Shaft Damage at Mohave Generating Station." Subsynchronous Resonance Symposium, IEEE Power Apparatus and Systems Summer Meeting, San Fransisco, California, 24 July 1975

[2] L.A. Kilgore, D.G. Ramey and M.C. Hall, "Simplified Transmission and Generation System Analysis Procedures for Subsynchronous Resonance Problems." IEEE Transactions on Power Apparatus and Systems, vol. PAS-96, pp. 1840-1846, November/December 1977.

[3] H.W. Dommel and I.I. Dommel, "Electromagnetic Transients Program User's Manual." University of British Columbia, August 1978

[4] H. Barnes and S. Kearley, "The Measurement of the Impedance Presented to Harmonic Currents by Power Distribution Networks." presented at the International Conference on Electricity Distribution, Brighton, England, 1-5 June 1981.

[5] D. Crevier and A. Mercier, "Estimation of Higher Frequency Network Equivalent Impedances by Harmonic Analysis of Natural Waveforms." IEEE Transactions on Power Apparatus and Systems, vol. PAS-97, pp. 424-431, March/April 1978.

[6] K.E. Bollinger, R. Winsor and D. Cotcher, "Power System Identification Using Noise Signals." (SUMPWR 76 Abstr. A76 339-2); IEEE Transactions on Power Apparatus and Systems, vol. 76, p. 1761, November/December 1976.

[7] F.X. Macedo, "Monitoring of System Impedance Using Arc-Furnace Disturbances", Universities Power Engineering Conference (1981) Sheffield

[8] F.X. Macedo, "Power System Harmonic Impedance Measurement Using Natural Disturbances", UBV Proceedings of the Third International Conference, London, May 1982

[9] D. Crevier, A Mercier, "Estimation of Higher Frequency Network Equivalent Impedances by Harmonic Analysis of Natural Waveforms", IEEE Transactions on Power Apparatus and Systems, vol. PAS-97, no. 2, March/April 1978.

[10] E. Clarke, "Circuit Analysis of A-C Power Systems, Volume 1." General Electric Company; Schenectady, New York; March 1961.

[11] B.P. Lathi, "Signals, Systems and Communication." John Wiley & Sons, New York, 1968

[12] T. Sugiyama, T. Nishiwaki, S. Takeda and S. Abe, "Measurements of Synchronous Machine Parameters Under Operating Condition." IEEE Transactions on Power Apparatus and Systems, vol. PAS-101, pp. 895-904, April 1982.

[13] R.P. Schulz, C.E.J. Bowler and W.D. Jones, Discussion on "Generator Models Established by Frequency Response Tests on a 555 MV.A Machine."

IEEE Transactions on Power Apparatus and Systems, vol. PAS-91, pp. 2077-2084, September/October 1972.

[14] K.C. Lee, "Propagation of the Wave Front On Untransposed Overhead and Underground Transmission Lines." M.A.Sc. Thesis, Electrical Engineering, University of British Columbia, April 1977

[15] General Electric, "Electrical Utility System Engineering Seminar - Subsynchronous Resonance." San Diego, California, August 1977

[16] Dr. A.S. Morched, "Verification of the Frequency Domain Technique for Calculating Asymmetrical Fault Currents", Ontario Hydro, March 1984

[17] Dr. A.S. Morched, Private Communication, November 1984

[18] J.H. Sawada and M. Scott, "General Power System Network Thevenin Equivalent Impedance Calculations Using Perturbation Method and Comparisons of Impedances Derived from Field Measurement and EMTP Model." B.C. Hydro Internal Report, 18 October 1984

[19] A. Clerici and L. Marzio, "Coordinated Use of TNA and Digital Computer for Switching-Surge Studies: Transient Equivalent of a Complex Network." IEEE Transactions on Power Apparatus and System, vol. PAS-89, pp. 1717-1726, November/December 1970

[20] A.S. Morched and V. Brandwajn, "Transmission Network Equivalents for Electromagnetic Studies." IEEE Transactions on Power Apparatus and System, vol. PAS-102, pp. 2984-2994, September 1983.

APPENDIX I - Derivation of Zpos(jw) for a Three Phase System

In phase quantities, the quantities in Figure 4 are related by the matrix equation:

$$[V] = [E] - [Z]\,[I]$$

To convert to symmetrical component quantities, pre-multiply by the sequence transformation matrix [S].

$$[S][V] = [S][E] - [S][Z][I]$$

Note that for a phase A to B fault the symmetrical component transformation is with phase C as reference. The transformation matrix [S] and it's inverse $[S]^{-1}$ are:

$$[S] = \frac{1}{3}\begin{bmatrix} 1 & 1 & 1 \\ a^2 & a & 1 \\ a & a^2 & 1 \end{bmatrix} \quad \text{and} \quad [S]^{-1} = \begin{bmatrix} 1 & a & a^2 \\ 1 & a^2 & a \\ 1 & 1 & 1 \end{bmatrix}$$

where $a = e^{-j120}$

In order to express the current in symmetrical component quantities, post-multiply [Z] by the identity $[1] = [S]^{-1}[S]$.

$$[S][V] = [S][E] - [S][Z][S]^{-1}\,[S][I]$$

$$[V_{sym}] = [E_{sym}] - [Z_{sym}]\,[I_{sym}]$$

If we assume a balanced system, then the symmetrical component impedance matrix will be:

$$[Z_{sym}] = \begin{bmatrix} Z_0 & 0 & 0 \\ 0 & Z_1 & 0 \\ 0 & 0 & Z_2 \end{bmatrix}$$

where: Z_0 = zero sequence impedance
Z_1 = positive sequence impedance, and
Z_2 = negative sequence impedance.

Converting back to phase quantities, by pre-multiplying with $[S]^{-1}$, we get:

$$[S]^{-1}[V_{sym}] = [S]^{-1}[E_{sym}] - [S]^{-1}[Z_{sym}]\ [I_{sym}]$$

$$[S]^{-1}[V_{sym}] = [S]^{-1}[E_{sym}] - [S]^{-1}[Z_{sym}][S]\ [S]^{-1}[I_{sym}]$$

$$[V] = [E] - [S]^{-1}[Z_{sym}][S]\ [I]$$

Substituting the current vector for a phase A to B fault:

$$\begin{bmatrix} V_a \\ V_b \\ V_c \end{bmatrix} = \begin{bmatrix} E_a \\ E_b \\ E_c \end{bmatrix} - \frac{1}{3} \begin{bmatrix} 1 & a & a^2 \\ 1 & a^2 & a \\ 1 & 1 & 1 \end{bmatrix} \begin{bmatrix} Z_0 & 0 & 0 \\ 0 & Z_1 & 0 \\ 0 & 0 & Z_2 \end{bmatrix} \begin{bmatrix} 1 & 1 & 1 \\ a^2 & a & 1 \\ a & a^2 & 1 \end{bmatrix} \begin{bmatrix} -I_f \\ I_f \\ 0 \end{bmatrix}$$

Calculating the voltage across the fault, $V_a - V_b$, yields:

$$(V_a - V_b) = (E_a - E_b) + (Z_1 + Z_2)\ I_f$$

$$\text{or} \quad V_{ab} = E_{ab} + (Z_1 + Z_2)\ I_f$$

Finally, defining $V_f = V_{ab} - E_{ab}$ and assuming $Z_1 = Z_2$, then:

$$Z_1 = \frac{1}{2}\ \frac{V_f}{I_f}$$

APPENDIX II - Fourier Transform Calculation

For a given time domain signal, say $v_f(t)$, we can obtain its frequency domain representation $V_f(jw)$ by using the general form of the Fourier transform,

$$V_f(jw) = \int_{-\infty}^{+\infty} v_f(t)\, e^{-jwt} dt$$

Assuming $v_f(t)$ is zero outside the time period of interest ($0<t<T$) and separating the real and imaginary components:

$$\mathrm{Re}\{V_f(jw)\} = A(jw) = \int_0^T v_f(t) \cos wt \, dt$$

$$\mathrm{Im}\{V_f(jw)\} = B(jw) = \int_0^T v_f(t) \sin wt \, dt$$

If the input quantity $v_f(t)$ is known at closely spaced discrete time intervals between 0 and T, and it is reasonable to assume linear interpolation between data points, then the equation for $v_f(t)$ between two adjacent points t1 and t2 is:

$$v_f(t) = v_1 + \frac{v_2 - v_1}{\Delta t} (t - t_1) \qquad \text{for } t_1 < t < t_2 \text{ and } \Delta t = t_2 - t_1$$

Substituting this into the equations for $V_f(jw)$ we get:

$$A_{12}(jw) = \int_{t_1}^{t_2} \left[v_1 + \frac{v_2 - v_1}{\Delta t} (t - t_1)\right] \cos wt \; dt$$

$$= \left[v_1 - \frac{v_2 - v_1}{\Delta t} t_1\right] \int_{t_1}^{t_2} \cos wt \, dt + \frac{v_2 - v_1}{\Delta t} \int_{t_1}^{t_2} t \cos wt \; dt$$

$$= \left[v_1 - \frac{v_2 - v_1}{\Delta t} t_1\right] \frac{1}{w} \sin wt \Big|_{t_1}^{t_2} + \frac{v_2 - v_1}{\Delta t} \frac{1}{w} \left(t \sin wt + \frac{1}{w} \cos wt\right) \Big|_{t_1}^{t_2}$$

$$= \frac{1}{w} \sin wt_2 \left[\left(v_1 + \frac{v_2-v_1}{\Delta t} t_2\right) - \frac{v_2-v_1}{\Delta t} t_1\right]$$

$$- \frac{\sin wt_1}{w} \left[\left(v_1 - \frac{v_2-v_1}{\Delta t} t_1\right) + \frac{v_2-v_1}{\Delta t} t_1\right] + \frac{v_2-v_1}{\Delta t w^2} (\cos wt_2 - \cos wt_1)$$

$$= \frac{1}{w} \left[v_2 \sin wt_2 - v_1 \sin wt_1 + \frac{v_2-v_1}{\Delta t w} (\cos wt_2 - \cos wt_1)\right]$$

Similarly for the imaginary component, B_{12}, we get:

$$B_{12}(jw) = \frac{1}{w} \left[-v_2 \cos wt_2 + v_1 \cos wt_1 + \frac{v_2-v_1}{\Delta t w} (\sin wt_2 - \sin wt_1)\right]$$

The calculations for $A_{12}(jw)$ and $B_{12}(jw)$ are repeated for all adjacent time samples over the entire time period under study ($0<t<T$). The real and imaginary part of the input quantity v(t) in the frequency domain at any specific frequency w is then the sum of all $A_{12}(jw)$'s and $B_{12}(jw)$'s, i.e.:

$$V(jw) = A(jw) + jB(jw)$$

$$= \sum_{k=0}^{T/\Delta t} A_{k,k+1}(jw) + jB_{k,k+1}(jw)$$

The above calculations are then repeated over the frequency range of interest (in this case $0<w<377$ rad/sec. or $0<f<60$ Hz) with whatever resolution, Δw, is desired. This result is then the Fourier transform of v(t), V(jw).

APPENDIX III - Time Domain Window to Eliminate Gibbs Oscillations

As derived so far, $V_f(jw)$ is actually the Fourier transform of $v_f(t)$ multiplied by the gate function g(t).

$$V_f(jw) = F\{v_f(t) \times g(t)\}$$

where $g(t) = 1$ for $-T/2 < t < T/2$
$= 0$ elsewhere

$$V_f(jw) = F\{v_f(t)\} * F\{g(t)\}$$

$$= F\{v_f(t)\} * Sa[wT/2]$$

where $Sa[x] = (\sin x)/x$ is the Sampling function. The calculated $V_f(jw)$ is therefore equal to the real Fourier transform of $v_f(t)$ convolved with the Sampling function $Sa[wT/2]$.

It can be seen from Figure 13 that $Sa[wT/2]$ has a major lobe at $w = 0$ and side lobe that oscillate with a period of $2Pi/T$ (radians/sec.) in the frequency domain. These side lobes of $F\{g(t)\}$ are what cause the Gibbs oscillation in $V_f(jw)$ and the Gibbs oscillation has this same period. In order to reduce the Gibbs oscillation $V_f(jw)$ can be averaged over the period $+/-Pi/T$ (radians/sec.) to develop an improved $V_f(jw)$ defined as $V'_f(jw)$.

$$V'_f(jw) = \frac{T}{2Pi} \int_{w-Pi/T}^{w+Pi/T} V(jv)\, dv$$

$$= \frac{T}{2Pi} \int_{w-Pi/T}^{w+Pi/T} \left(\int_{-T/2}^{T/2} f(t)\, e^{-jvt}\, dt \right) dv$$

$$= \frac{T}{2Pi} \int_{-T/2}^{T/2} f(t) \left(\int_{w-Pi/T}^{w+Pi/T} e^{-jvt} dv \right) dt$$

$$= \frac{T}{2\ Pi} \int_{-T/2}^{T/2} f(t) \left[\frac{e^{-jvt}}{-jt} \right]_{w-Pi/T}^{w+Pi/T} dt$$

$$= \int_{-T/2}^{T/2} f(t) \frac{\sin(Pi\ t/T)}{(Pi\ t/T)} e^{-jwt}\ dt$$

$$= \int_{-T/2}^{T/2} f(t)\ Sa(Pi\ t/T)\ e^{-jwt}\ dt$$

This averaging of $V_f(jw)$ over the period of the Gibbs oscillation can therefore be achieved by simply multiplying (gating) $v_f(t)$ by Sa[Pi t/T] over the range $-T/2 < t < T/2$. This new shape of gate function is the major lobe of Sa[Pi t/T] which goes smoothly to zero at the end of the time sample - i.e. t = +/- T/2. The time signal $v_f(t)$ is therefore gradually attenuated to zero so that no truncation, and Gibbs oscillations, occurs.